NASA TECHNICAL NOTE

NASA TN D-4659

NASA TN D-4659

c. 1

ANALYSIS OF RADIATOR CHARACTERISTICS OF A SINGLE-LOOP 100-KILOWATT BRAYTON SPACE POWER SYSTEM USING A PURE GAS AND A GAS-SOLID SUSPENSION

by

Robert Pfeffer and Salvatore Rossetti
City College of the City University of New York

and

Seymour Lieblein
Lewis Research Center

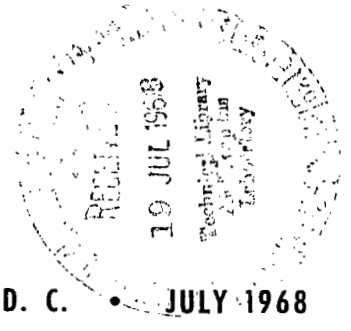

NATIONAL AERONAUTICS AND SPACE ADMINISTRATION • WASHINGTON, D. C. • JULY 1968

ANALYSIS OF RADIATOR CHARACTERISTICS OF A SINGLE-LOOP 100-KILOWATT BRAYTON SPACE POWER SYSTEM USING A PURE GAS AND A GAS-SOLID SUSPENSION

By Robert Pfeffer and Salvatore Rossetti

City College of the City University of New York
New York, New York

and

Seymour Lieblein

Lewis Research Center
Cleveland, Ohio

NATIONAL AERONAUTICS AND SPACE ADMINISTRATION

For sale by the Clearinghouse for Federal Scientific and Technical Information
Springfield, Virginia 22151 – CFSTI price $3.00

ABSTRACT

Results are presented for an exploratory comparative analysis of radiator geometric characteristics based on a simplified radiator model with either a pure gas or a graphite-gas suspension working fluid. Radiator variables investigated were gas-flow Reynolds number, pressure-drop fraction, and suspension-particle loading ratio. For the pure gases, type of gas and Reynolds number had a pronounced effect on tube and panel geometry, but Reynolds number and pressure drop fraction had a relatively small effect on planform area for fixed overall cycle loss pressure ratio. Only moderate reductions in radiator planform area (10 to 17 percent) were indicated with the use of graphite-gas suspensions.

STAR Category 03

CONTENTS

ANALYSIS OF RADIATOR CHARACTERISTICS OF A SINGLE-LOOP 100-KILOWATT BRAYTON SPACE POWER SYSTEM USING A PURE GAS AND A GAS-SOLID SUSPENSION

by Robert Pfeffer,* Salvatore Rossetti,† and Seymour Lieblein

SUMMARY

An exploratory comparative analysis of radiator characteristics for a 100-kilowatt single-loop Brayton space power cycle has been conducted based on a simplified radiator model in which either a pure gas or a graphite-gas suspension was used as the working fluid. Gases considered were helium, neon, and argon, with parametric variations of gas-flow Reynolds number, overall cycle loss pressure ratio, fractional pressure drop across the radiator, and suspension-particle loading ratio. Recently developed correlations were used for the required properties of the gas-solid suspension. Outputs of the calculations were optimum cycle temperature ratios, radiator planform area, tube geometry (number, length, and inner diameter), panel planform area, and optimum suspension-particle loading ratio. In addition, an approximate radiator weight comparison was provided for the suspension cases.

The principal results of the analysis for the assumptions and conditions covered indicated that, for the pure-gas working fluids, the gas Reynolds number and radiator pressure-drop fraction had a relatively small effect on radiator planform areas as long as the overall cycle loss pressure ratio was kept constant. However, even at a constant cycle loss pressure ratio, type of gas and Reynolds number had a prounced effect on the radiator tube and panel geometry.

Moderate reductions in radiator planform area compared with the pure-gas case were obtained, with the use of a graphite-gas suspension, with an average reduction of 17 percent for helium, 13.5 percent for neon, and 10.5 percent for argon. Somewhat larger reductions in weight were indicated by the approximate weight analysis, with magnitude depending on the basis of comparison between the pure-gas and suspension cases. It was concluded that a more precise evaluation of the potential reduction in radiator area and weight achievable with the use of a solid suspension would require more accurate property data for particle suspensions at low loading ratios and more sophisticated radiator analyses.

---

*Associate Professor, City College of the City University of New York.

†Graduate Student, City College of the City University of New York.

INTRODUCTION

Advanced space-power generation systems must be able to continuously supply electrical power for long periods of time. One such power generating system currently under technical evaluation is the indirect conversion, closed-loop heat engine based on the Brayton cycle. In this system, heat is generated in a nuclear or solar source and rejected by a radiator, with power being obtained from a turbine located in the working fluid cycle.

Several analyses of potential performance of a Brayton cycle using an inert gas as the working fluid have been conducted (refs. 1 to 4). These studies have indicated that, because of the relatively low temperature levels in the radiator and the inherently low heat-transfer coefficients of gases, the Brayton-cycle waste-heat rejection structure in a single-loop system is relatively large and heavy.

One method of decreasing the radiator area, and hence its weight, in a single-loop system is to increase the heat-transfer coefficient of the gas working fluid, thus allowing greater heat transfer per unit of radiation area. For a pure gas working fluid, the heat-transfer coefficient is governed by the Reynolds number of the flowing fluid, which, in turn, is related to the geometric characteristics of the radiator.

Decreasing the pressure drop through the heat-transfer components of the cycle is still another way to decrease the area and weight of the system. Reductions in pressure drop will increase the cycle efficiency, which, in turn, causes a reduction in the required radiator area. Here too, the radiator flow Reynolds number is a prime influencing factor.

Another possibility would be to decrease the isentropic specific-heat ratio of the working fluid. A decrease in the specific-heat ratio of the fluid results in a higher thermal efficiency for the Brayton cycle and hence a lower required radiator area (ref. 6). It has been shown (ref. 5) that the addition of small particles to a gas will produce a substantially lower isentropic heat-capacity ratio than that of the pure-gas component. A gas-solid suspension will also increase the heat-transfer coefficient of the flowing fluid (ref. 5). Thus, the use of a gas-solid suspension as the working fluid in a single-loop Brayton cycle may have a potentially advantageous effect on the cycle heat-rejection system. A preliminary analysis of such a cycle, based on suspension-property assumptions and simplified conditions made in reference 6, indicated a large reduction in radiator area.

A rigorous parametric study of the effects of such factors as gas-flow Reynolds number, pressure loss, and particle addition on the geometric characteristics of a Brayton cycle radiator over wide ranges of variation is a cumbersome task in view of the complex nature of the design procedures for a gas radiator (e.g., ref. 7). However, if a valid simplified radiator model is used, an analysis procedure can be developed that

can provide first-order or preliminary comparative information with only a moderate calculation effort.

This report presents the development and method of solution for a combination cycle analysis and radiator model that can be used to determine the preliminary geometric characteristics of radiator designs using either a pure gas or a gas-solid suspension as the working fluid. The effects of pertinent variables such as gas-flow Reynolds number, pressure loss through the radiator, and the properties of the pure gas or gas-solid suspension on the radiator design are determined and compared over a wide range of variables. The calculations are made for the specific case of a representative 100-kilowatt-output power cycle with fixed maximum temperature and fixed component efficiencies. Argon, neon, and helium are considered for the cycle working fluid, and graphite is considered as the suspension particle material.

THERMODYNAMIC ANALYSIS

A schematic flow diagram of a single-loop Brayton cycle is shown in figure 1. The numbers correspond to the state-point designation used in this analysis. The gas leaving the heat source at point 1 expands through the turbine to point 2, thereby producing the mechanical work necessary to drive the compressor and alternator. From the turbine the gas enters the recuperator where it is cooled to point 3, as it transfers heat to

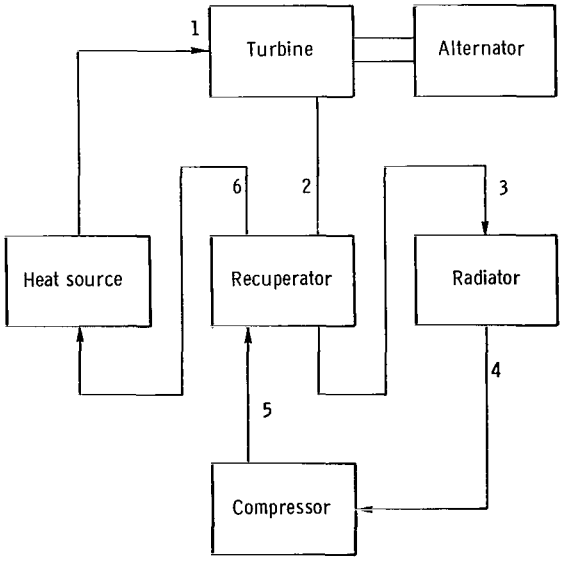

Figure 1. - Flow diagram of single-loop Brayton cycle. (Numbers denote state-points.)

the gas leaving the compressor. Final cooling to point 4 takes place in the radiator where the excess heat is rejected to space. The gas leaving the radiator is then compressed to point 5, heated in the recuperator to point 6, and further heated back to point 1 in the heat source.

Equations for calculating the thermodynamic cycle efficiency η_{cy}, the working fluid flow rate W, and the prime radiating area A_p (symbols are defined in appendix A) of the Brayton cycle shown in figure 1 have been developed in reference 1 and are presented in appendix B. The prime radiating area A_p in equation (B4) is defined as the area of either a tubular radiator without fins or a fin-and-tube radiator with 100-percent fin efficiency. It is the minimization of this area which is generally used as a criterion for optimum cycle temperature selection. The prime area is an acceptable preliminary criterion for the evaluation and comparison of radiator characteristics because it can be obtained analytically in a simple manner, is proportional to radiator weight and size (radiator planform area), and minimizes at approximately the same cycle temperatures as the full size and weight of a fin-and-tube radiator (ref. 7).

Examination of the equations of appendix B indicates that, for fixed cycle power output P_s, maximum temperature T_1, space sink temperature T_s, and component efficiencies η_C, η_T, and E, the prime radiating area will be determined by the fluid isentropic specific-heat ratio γ, the radiator heat-transfer coefficient h_R, the cycle loss pressure ratio r_T/r_C, and the temperature ratios T_2/T_1 and T_4/T_1. The values of the last two quantities are generally selected according to some cycle design criterion (i.e., minimum prime area), so that they become secondary variables. Thus, the primary factors of interest in determining radiator characteristics are r_T/r_C, h_R, and γ.

The cycle loss pressure ratio r_T/r_C defined as the ratio of turbine inlet to exit pressure divided by the ratio of compressor exit to inlet pressure, is also equal to the product of the ratios of exit to inlet pressure for all the heat-transfer components. Consequently, r_T/r_C represents the fraction of compressor pressure ratio that can be recovered to do the work in the turbine and is an indicator of the cumulative pressure drops of the heat-transfer components. Prime radiating area is very sensitive to the value of the cycle loss pressure ratio (e.g., ref. 1). Therefore, the effect of the contribution of the pressure drop through the radiator to the overall loss is an important factor for consideration.

Another important parameter necessary to determine the prime radiating area is the gas film or inside-surface convective heat-transfer coefficient h_i. This quantity is related to the radiator heat-transfer coefficient h_R, which is required in computing the prime radiating area (eq. (B4)) by the relation

$$h_R = \frac{h_i A_i}{A_p} \tag{1}$$

where A_i is the inside surface area of the tube and A_p is the prime radiating area. References 1 to 3 assumed h_R to be an independent parameter that was held constant in the cycle calculations. It is known, however, that h_i is dependent on gas Reynolds number, tube diameter, and fluid properties. This is especially true if a gas-solid suspension is used as the working fluid, because h_i will depend strongly on the suspension properties. For these reasons, h_R will not be assumed constant but will be computed in the cycle analysis for different conditions and different working fluids.

The specific heat C_p has a unique value for a pure gas at a given temperature. However, for a gas-solid suspension, the value of the specific heat will depend on the specific heats of the carrier gas and the particle and the particle loading ratio η, defined as the ratio of the mass flow rate of solid particles to that of the pure gas,

$$\eta = \frac{w_p}{w_g} \tag{2}$$

The specific heat of the suspension is given by (ref. 5)

$$\left(C_p\right)_s = \left(C_p\right)_g \frac{1 + \delta\eta}{1 + \eta} \tag{3}$$

where δ is defined as the ratio of specific heat of the particles to that of the pure gas

$$\delta = \frac{\left(C_p\right)_p}{\left(C_p\right)_g} \tag{4}$$

The specific heat of a gas-solid suspension can either be greater or smaller than the value for the carrier gas (ref. 5), but because the product wC_p appears as the variable affecting the prime area in equation (B4), the specific heat is not involved as a cycle parameter (eq. (B3)). However, the specific heat of the working fluid must be known in order to determine the mass flow rate w (eq. (B3)).

The proper value to be used for the isentropic heat ratio of a suspension γ_s is not as clearly defined as for the specific heat. If, however, equilibrium between gas and particles can be assumed that is, $T_p = T_g$ and $V_p = V_g$, then the isentropic specific-

heat ratio of a suspension γ_s in terms of the readily available properties of the system can be estimated by (ref. 5).

$$\gamma_s = \gamma_g\left(\frac{1 + \delta\eta}{1 + \gamma_g\delta\eta}\right) \tag{5}$$

For a suspension, the specific-heat ratio will be less than that of the carrier gas. For large suspension-particle loading ratios ($\eta > 10$), γ_s approaches 1.0, and the suspension behavior approaches that of an incompressible fluid.

The effect of a reduced isentropic specific-heat ratio γ on the thermodynamics of the Brayton cycle is to increase the cycle efficiency and hence reduce the heat rejection required by the radiator. The general sensitivity of the prime radiating area A_p to the isentropic specific-heat ratio is illustrated in figure 2 for representative cycle conditions and a fixed value of h_R. It should be noted, however, that a reduction in isentropic specific-heat ratio results in an increase in the pressure ratios across the turbine and

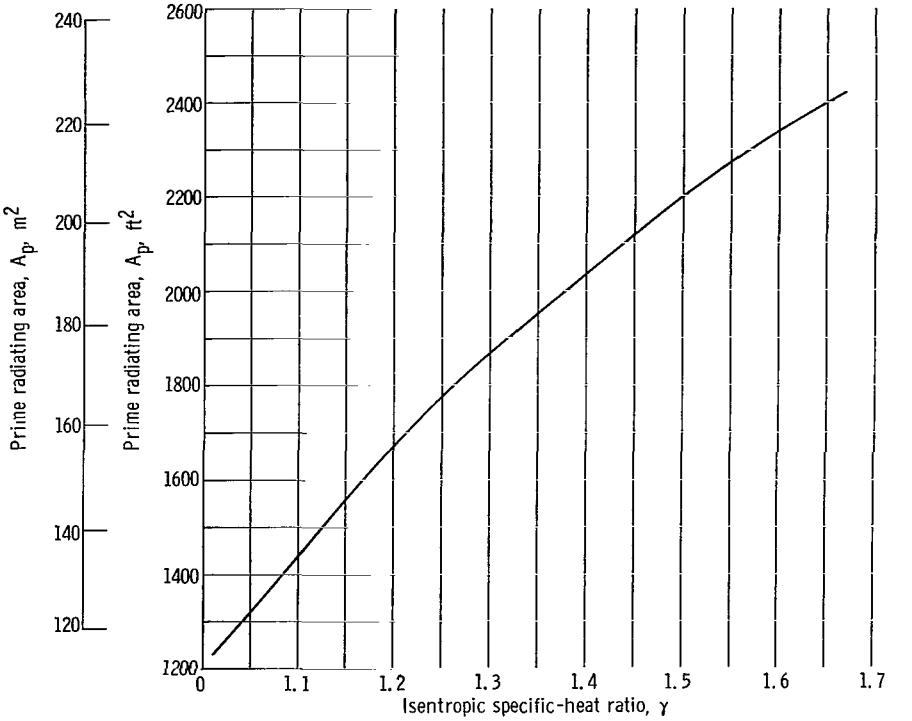

Figure 2. - Variation of minimum prime radiating area with isentropic specific-heat ratio. Inlet temperature, 2200° R (1220 K); turbine efficiency, 0.85; compressor efficiency, 0.80; convective heat-transfer coefficient, 10 Btu per hour per square foot per °F (56.8 W/(m^2)(K); recuperator effectiveness, 0.85; surface emissivity, 0.86; shaft power, 100 kilowatts.

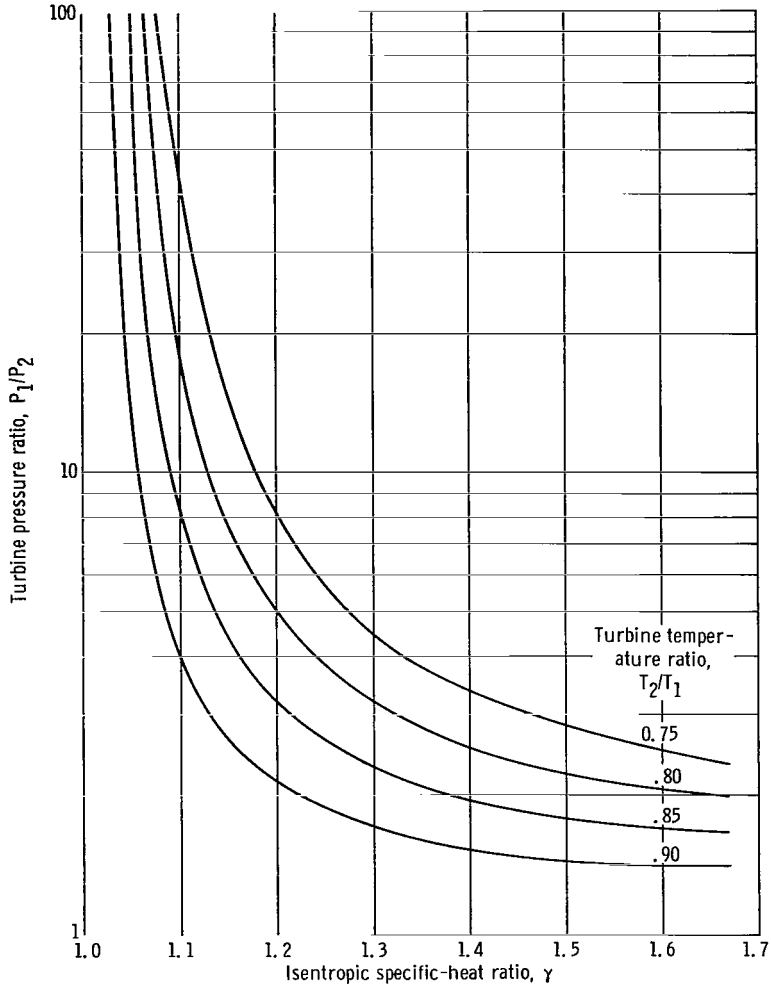

Figure 3. - Variation of turbine pressure ratio with isentropic specific-heat ratio, with turbine temperature ratio as parameter for fixed turbine efficiency of 0.85.

compressor for a given temperature ratio. This effect on the turbomachinery is illustrated in figure 3.

RADIATOR ANALYSIS

Radiator Configuration

The radiator configuration considered in the analysis (fig. 4) is one with a central fin-tube panel geometry of axial length L and N number of tubes. This configuration is composed of tubes of inside diameter D_i and outside diameter D_o and rectangular

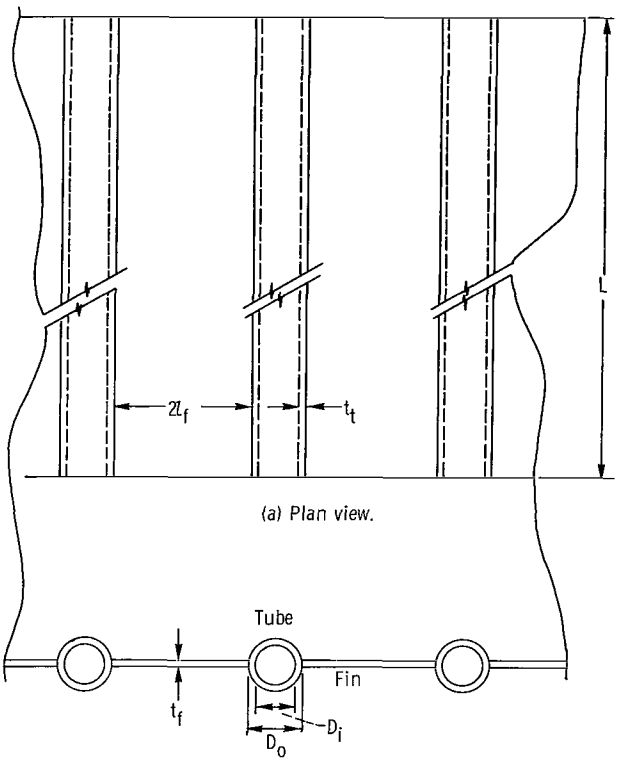

Figure 4. - Central fin-tube radiator configuration.

fins of thickness t_f and width $2l_f$. Heat rejection occurs from the outside surface of the tubes and from both surfaces of the fins by radiation to space. For simplicity, the headers are neglected, and only the fin tube panel is considered.

Preliminary design calculations of the 100-kilowatt single-loop Brayton cycle radiators based on a comprehensive computer program (ref. 7) had indicated that, for tube inside diameters larger than around 3/8 to 1/2 inch (0.95 to 1.27 cm), the ratio of fin half width to tube outside diameter l_f/D_o, and the overall radiating effectiveness η_f showed little variation with tube inside diameter D_i and type of inert gas used for minimum-weight configurations. It was also acceptable to consider a constant average value of the ratio of tube outside to inside diameter D_o/D_i. The use of a constant value of D_o/D_i is consistent with internal pressure considerations and, in the more exact calculations, showed small effect on the variation of planform area with tube inside diameter. Thus, it was established that, for comparative analysis purposes, a simplified radiator fin tube model can be established based on representative constant values of l_f/D_o, η_f, and D_o/D_i that would produce radiator planform areas closely representative of those of minimum-weight radiators.

Based on this simplified model geometry, equations will now be written that determine the radiator pressure relations, heat-transfer rate, and radiator panel geometry.

Pressure Relations

In order to be able to investigate the effect of the pressure drop through the radiator on the cycle, it is necessary to analyze the pressure drops through all the heat-transfer components in relation to the cycle loss pressure ratio. The cycle loss pressure ratio and the pressure at various points in the cycle can be expressed in terms of the pressure drop across the radiator $(\Delta P)_{rad}$. The development of these equations is given in appendix C. From these derivations, it is shown that,

$$\frac{r_T}{r_C} = \frac{1 - \left(\frac{1}{1 - K_2}\right)\left[\frac{(\Delta P)_{rad}}{P_1}\right]\frac{P_1}{P_2}}{1 + \left(\frac{1}{K_1} - \frac{K_2}{1 - K_2} - 1\right)\left[\frac{(\Delta P)_{rad}}{P_1}\right]} \tag{6}$$

where K_1 is defined as the ratio of the pressure drop in the radiator to the total system pressure drop,

$$K_1 \equiv \frac{(\Delta P)_{rad}}{(\Delta P)_{tot}} \tag{7}$$

and K_2 is defined as the ratio of the pressure drop in the low-pressure side of the recuperator to the total pressure drop in the cold side of the cycle (radiator and recuperator), or

$$K_2 \equiv \frac{(\Delta P)_{rec}}{(\Delta P)_c} = \frac{P_2 - P_3}{P_2 - P_4} \tag{8}$$

In the analysis, K_1 and K_2 are taken as independent parameters, within certain bounds (see appendix C), and P_1 is considered to be fixed. The turbine pressure ratio P_1/P_2 is given by

$$\frac{P_1}{P_2} = \left[1 - \frac{1}{\eta_T}\left(1 - \frac{T_2}{T_1}\right)\right]^{-(\gamma/\gamma-1)} \tag{9}$$

Equations for the total pressure at all cycle stations in terms of the preceding variables are also derived in appendix C.

The cycle loss pressure ratio can also be expressed in terms of the radiator pressure-drop parameters and a fixed value of the total pressure loss in all the cycle components except the radiator $(\Delta P)_{comp}$. This expression (eq. (C18)) is

$$\frac{r_T}{r_C} = \frac{(1 - K_2)\left(\frac{1 - K_1}{K_1}\right) - \frac{P_1}{P_2}\left[\frac{(\Delta P)_{comp}}{P_1}\right]}{(1 - K_2)\left(\frac{1 - K_1}{K_1}\right)\left[1 + \frac{(\Delta P)_{comp}}{P_1}\right] - K_2\left[\frac{(\Delta P)_{comp}}{P_1}\right]} \tag{10}$$

The radiator pressure drop can then be related to the radiator geometry, the fluid properties, and the cycle mass flow rate (appendix C) as

$$(\Delta P)_{rad} = 2F\left[1 + 4.0(Re)_g^{-0.32}\eta\right]\left[0.046(Re)_g^{-0.2}\right]\left(\frac{L}{D_i}\right)\left(\frac{R'T_3}{g_c P_3}\right)\left[\frac{w_s}{(1 + \eta)\frac{\pi}{4} D_i^2 N}\right]^2 \tag{11}$$

where

$$F = 1.5\left[\frac{1 - \left(\frac{T_3}{T_4}\right)^2}{1 - \left(\frac{T_3}{T_4}\right)^3}\right] \tag{12}$$

and

$$(Re)_g = \frac{w_s}{\mu(1 + \eta)\frac{\pi}{4} D_i N} \tag{13}$$

For the pure gas, $\eta = 0$, and $w_s = w_g$. Thus additional equations are required to relate the geometric parameters of the radiator (N, D_i and L).

Heat-Transfer Coefficient

Although previous cycle analyses assumed a constant value for the heat-transfer coefficient related to radiating area h_R (eq. (1)), in the calculation of A_p (eq. (B4)), the use of the radiator model allows for the calculation of this factor for different gases (or gas-solid suspensions), different flow conditions, and different temperatures and pressures. The heat-transfer coefficient between the gas and the tube inner surface h_i, can be computed for a pure gas from the relation (ref. 8)

$$h_g = 0.023\left(\frac{k_g}{D_i}\right)(Re)_g^{0.8}(Pr)_g^{0.3} \tag{14}$$

where $(Re)_g$ is given by equation (13) for $\eta = 0$ and $w_s = w_g$, and

$$(Pr)_g = \frac{\left(C_p\right)_g \mu_g}{k_g} \tag{15}$$

Reference 5 has shown that the relation between h_s, the heat-transfer coefficient of a gas-solid suspension, and h_g, the heat-transfer coefficient of a pure gas, can be taken as

$$\frac{h_s}{h_g} = \left[1 + 4.0(Re)_g^{-0.32}\,\delta\eta\right] \tag{16}$$

so that, for the case of a suspension flow,

$$h_s = \frac{0.023\,k_g(Re)_g^{0.8}}{D_i}\left(\frac{\left(C_p\right)_g \mu_g}{k_g}\right)^{0.3}\left[1 + 4.0(Re)_g^{-0.32}\,\delta\eta\right] \tag{17}$$

The values of h_i, using either equation (13) for the pure-gas equation, or equation (17) for the gas-solid suspension, are converted to h_R by equation (1) where the

tube inside surface area is

$$A_i = \pi D_i LN \tag{18}$$

The prime radiating area A_p is obtained directly from the cycle analysis as indicated in equation (B4). It now remains to relate the calculated prime area to the geometry of the radiator model.

The total radiating surface area A_R of the radiator model (fig. 4) is given by

$$A_R = 2D_o\left(\frac{\pi}{2} + 2\frac{l_f}{D_o}\right)LN \tag{19}$$

The prime area, which is the effective radiating area, will differ from the total radiating area as given by equation (19) because of two factors: (1) The fins are not radiating at 100-percent efficiency, and (2) some of the radiation leaving the radiator surface is intercepted by some other part of the surface (i.e., the view factor to space is less than one).

The first factor can be accounted for by correcting the fin radiating area by a factor less than 1.0 (the fin efficiency). Reference 9 has shown that the second factor can be corrected by using the projected area of the tubes $2D_oLN$ rather than the actual radiating area πD_oNL. The prime (or effective) radiating area can therefore be described by

$$A_p = 2D_oNL + 4\eta_f\left(\frac{l_f}{D_o}\right)D_oLN \tag{20}$$

so that, in terms of D_i,

$$A_p = 2D_i\left(\frac{D_o}{D_i}\right)\left(1 + 2\eta_f\frac{l_f}{D_o}\right)LN \tag{21}$$

Therefore, from equations (18) and (21)

$$\frac{A_i}{A_p} = \frac{1}{\frac{D_o}{D_i}\left(\frac{2}{\pi} + \frac{4}{\pi}\eta_f\frac{l_f}{D_o}\right)} \tag{22}$$

so that equation (1) becomes,

$$h_R = \frac{h_i}{\frac{D_o}{D_i}\left(\frac{2}{\pi} + \frac{4}{\pi}\eta_f \frac{l_f}{D_o}\right)} \tag{23}$$

The use of either equation (14) or (17) for h_i requires an expression for the tube inside diameter D_i. This relation is obtained by combining equations (11) and (13) to give

$$D_i = \sqrt[3]{\frac{(Re)_g^2}{\Delta P_{rad}} 0.092(Re)_g^{-0.2}\left[1+4.0(Re)_g^{-0.32}\eta\right]\frac{LF\mu^2 R' T_3}{g_c P_3}}$$

An expression for the length of tubes L required in equation (24) can be obtained by combining equations (13) and (21) to yield,

$$L = \frac{A_p (Re)_g}{8 w_s} \frac{\mu\pi(1+\eta)}{\left(1 + 2\eta_f \frac{l_f}{D_o}\right)\frac{D_o}{D_i}} \tag{25}$$

Thus, if representative values of η_f, l_f/D_o, and D_o/D_i can be prescribed, equation (23) allows h_R to be related to gas properties and the radiator geometry.

Panel Geometry

The use of the simplified radiator model allows the calculation of significant features of the panel geometry such as the planform area, panel aspect ratio, and area vulnerable to meteoroid damage as functions of the tube flow Reynolds number, the fluid properties, and the cycle conditions.

The planform area is defined as the projected area of the radiator panel neglecting the headers, and is described by

$$A_{pl} = NLD_o\left(1 + 2\frac{l_f}{D_o}\right) \tag{26}$$

where the number of tubes N is then obtained from equation (C40) as,

$$N = \frac{4w_s}{\pi G_g D_i^2 (1 + \eta)} \tag{27}$$

The planform area is related to the prime area by the ratio,

$$\frac{A_{pl}}{A_p} = \frac{\left(1 + 2\frac{l_f}{D_o}\right)}{2\left(1 + 2\eta_f \frac{l_f}{D_o}\right)} \tag{28}$$

The vulnerable area (area vulnerable to damaging impact by meteoroids) is

$$A_v = \pi D_o N L \tag{29}$$

so that in ratio form

$$\frac{A_v}{A_{pl}} = \frac{\pi}{\left(1 + 2\frac{l_f}{D_o}\right)} \tag{30}$$

Another significant factor considered in the design of radiators is the panel aspect ratio φ which is defined as the length-to-width ratio of the panel and is expressed as,

$$\varphi = \frac{L}{N(D_o + 2l_f)} = \frac{L^2}{A_{pl}} \tag{31}$$

CALCULATIONS

Method of Solution

Once the cycle parameters η_T, η_C, E, and r_T/r_C are specified and the independent variables T_2/T_1, T_4/T_1, P_1, and P_s are chosen, the cycle is fully described for a

given pure gas or a specified gas-solid suspension. From the cycle analysis, w, A_p, and all temperatures are determined. When the radiator model constants (D_o/D_i, l_f/D_o, η_f, K_1, and K_2) are fixed and the gas Reynolds number in the tubes of the radiator are prescribed, the four equations (13), (24), (25) and (27) in conjunction with the cycle outputs were used to determine the four parameters, D_i, G_g, L, and N, respectively. An iterative procedure was required based on an initial assumption of D_i due to the dependence of h_R (which is necessary for the cycle analysis) on D_i. All calculations were performed on an IBM 7094 computer. The computational procedure is presented in appendix D.

Inputs

The example chosen for the parametric analysis was a 100-kilowatt shaft power output cycle using either pure helium, neon, or argon, or a suspension of graphite in these gases as the working fluid. From turbomachinery considerations, compatible values of 2200° R (1222 K) and 25 200 pounds per square foot (12.1×10^4 N/m^2) chosen, respectively, as the turbine entering temperature T_1 and pressure P_1. The equivalent sink temperature was chosen as 400° R (222 K), and the value of 0.86 was chosen for the emissivity, ϵ, of the tubes and fins. Values of the compressor, turbine, and recuperator efficiencies were taken as 0.85 ($\eta_C = \eta_T = E = 0.85$) for both the pure gases and the gas-solid suspensions.

The three important cycle parameters are T_2/T_1, T_4/T_1, and the cycle loss pressure ratio, r_T/r_C. In this analysis, T_2/T_1 was varied between 0.70 and 0.90, and T_4/T_1 was varied between 0.25 and 0.45 in increments of 0.025. The allowable or design value of the cycle loss pressure ratio is generally a compromise between cycle efficiency and component flow passage size and weight. The best or optimum value can be determined from a complete system weight and performance analysis; it is not clear, beforehand, what an acceptable value might be. Much will depend on which components are most sensitive to size. In most cases, the principal components that are dependent on flow passage size are the heat source (e.g., reactor and shielding, radioisotope and shielding) and the radiator. In order to ascertain the effect of r_T/r_C on the radiator design, the cycle loss pressure ratio was taken as 0.85, 0.90, and 0.95 for the pure-gas analysis; whereas an average value of 0.90 was chosen for the gas-solid suspension studies.

As a parametric variable, the Reynolds number was chosen between 10 000 and 500 000 depending on the gas. The Reynolds number range for each gas was chosen to keep the tube inside diameter above 3/8 inch (0.95 cm) in order not to invalidate the model assumptions discussed previously. Based on the analyses of gas-cycle radiators,

representative geometric parameter values were selected as $D_o/D_1 = 1.33$, $l_f/D_o = 3.5$, and $\eta_f = 0.67$.

A constant value of 0.25 was considered appropriate for the recuperator pressure-drop fraction K_2. In order to test the sensitivity of the radiator design to the radiator pressure-drop fraction K_1, three values of K_1 (0.2, 0.5, and 0.75) were selected as input data for the pure gas studies. The value of $K_1 = 0.75$ is the limiting value of this parameter when $K_2 = 0.25$ if no pressure losses occur in either the high-pressure side of the recuperator or the heat source. For the gas-solid suspensions studies, a single value of $K_1 = 0.5$ was chosen.

The significance of the factor K_1 as a direct measure of the pressure drop through the radiator is illustrated in figures 5 and 6. Figure 5 shows the relation between the pressure drop through the radiator $((\Delta P)_{rad}/P_3)$ and K_1 for three different values of r_T/r_C for the case of $K_2 = 0.25$. The calculation was made for a value of $T_2/T_1 = 0.8$. It is seen that if the overall cycle loss pressure ratio is fixed, decreasing the value of K_1 will decrease the pressure drop in the radiator, but will also simultaneously increase the pressure drop in the other heat-transfer components.

In certain applications, it may be necessary to fix the pressure drop in the other heat-transfer components rather than the overall cycle loss pressure ratio. Figure 6

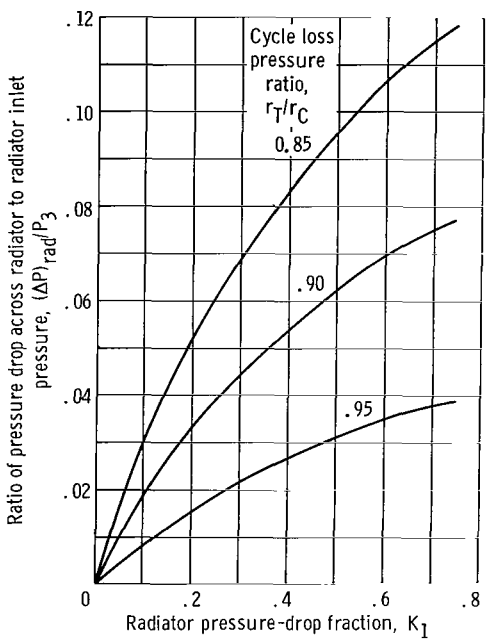

Figure 5. - Variation of ratio of pressure drop across radiator to inlet pressure with radiator pressure-drop fraction for fixed cycle loss pressure ratio. Recuperator pressure-drop fraction, 0.25; outlet-inlet turbine temperature ratio, 0.8.

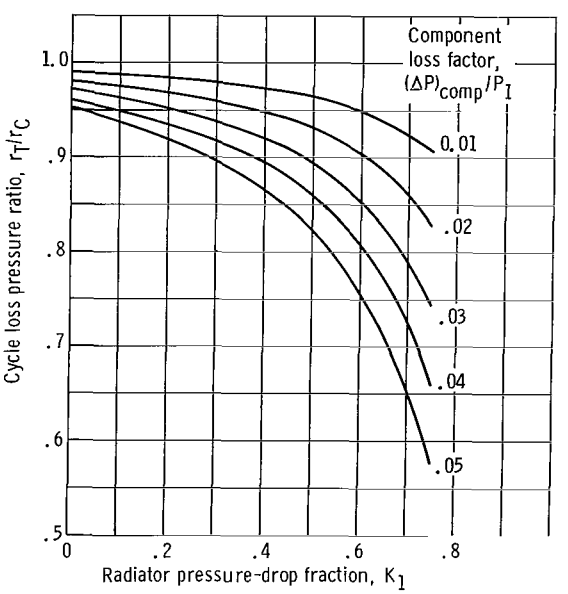

Figure 6. - Variation of cycle loss pressure ratio with radiator pressure-drop fraction. Recuperator pressure-drop fraction, 0.25; outlet-inlet turbine temperature ratio, 0.8.

shows the relation between the cycle pressure ratio and K_1 for $K_2 = 0.25$ for five different values of the total pressure drop in the other heat-transfer components, $(\Delta P)_{comp}/P_1$ (eq. (10)). Thus, if the total pressure drop in the other heat-transfer components is specified (with $K_2 = 0.25$), figure 6 can be used to choose a value of K_1 which will result in an acceptable value of the overall cycle loss pressure ratio. If, on the other hand, all three individual pressure drops comprising $(\Delta P)_{comp}$ are specified, the values of K_1 and K_2 can be calculated directly from equations (7) and (8), and the operating cycle loss pressure ratio is obtained from equation (10).

The pure gases that were considered are the inert gases: helium, neon, and argon. The properties of these gases required as inputs to the analysis were thermal conductivity k, viscosity μ, specific heat C_p, isentropic specific heat ratio γ, and gas constant R'. Values of these properties for the temperature range of interest are presented in appendix E. The gas-solid suspensions studied were suspensions of graphite in these same inert gases. The pertinent physical properties of graphite are also presented in appendix E.

RESULTS AND DISCUSSION

The geometric parameters of the radiator were computed for each gas and suspension case as a function of the temperature ratios T_2/T_1 and T_4/T_1. Radiator planform area was used as the principal output factor, and the minimum value of the planform area was selected as the criterion for the optimum cycle temperature ratio. Once the optimum temperature ratios were established, a parametric analysis of the important variables affecting the radiator geometry at these temperatures was made possible. These variables include the inert gas to be used as the working fluid, the suspension-particle loading ratio, the gas Reynolds number, the cycle loss pressure ratio, and the radiator pressure-drop fraction K_1.

Although radiator planform area is taken as a principal measure of radiator performance in view of its direct relation to radiator weight and size, it should be noted that variations in prime and vulnerable area can also be determined from applications of equations (28) and (31).

Pure-Gas Results

Optimum temperature ratios. - A typical plot of the planform area A_{pl} against T_2/T_1 with T_4/T_1 as a parameter is presented in figure 7 for neon. Although a minimum value of temperature ratio is indicated in all cases, the plot shows that the curves

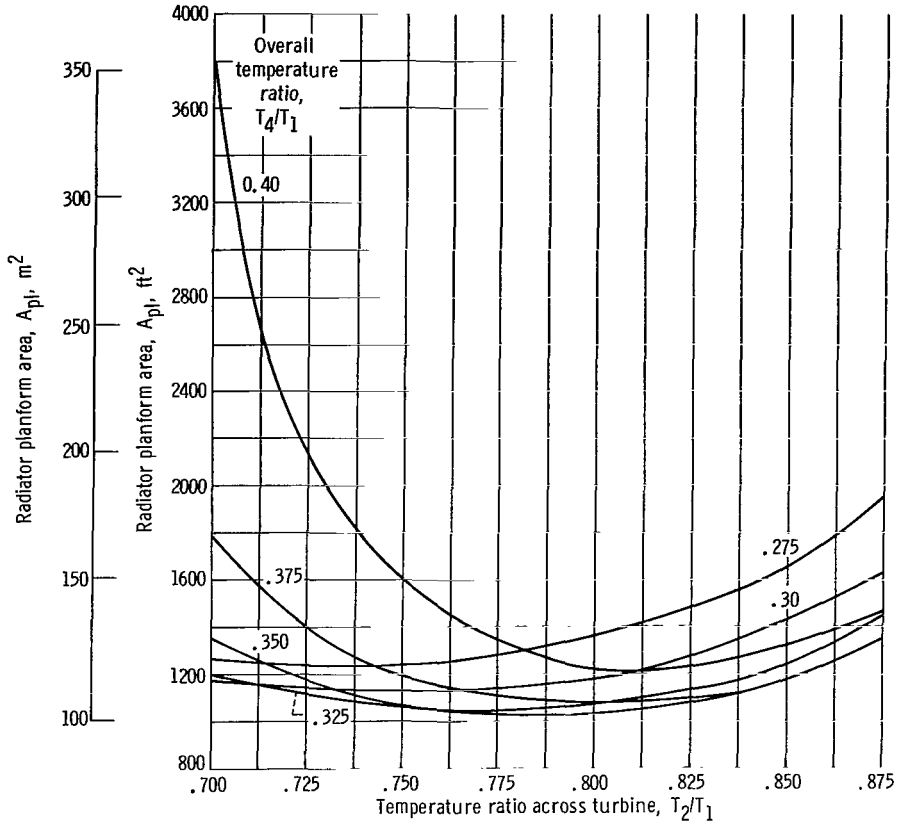

Figure 7. - Variation of radiator planform area with temperature ratio across turbine for 100-kilowatt neon cycle. Gas Reynolds number, 50 000; cycle loss pressure ratio, 0.90; radiator pressure-drop fraction, 0.5; recuperator pressure-drop fraction, 0.25.

are fairly shallow in the vicinity of the minimum. In general, the optimum temperature conditions (T_2/T_1 and T_4/T_1) were obtained in the analysis by scanning the computer output for the smallest value of A_{pl} and not by plotting the planform area. The increment used for varying T_2/T_1 and T_4/T_1 in the computer program was quite small (±0.025) so that the maximum error from this procedure would be ±0.025 in the temperature ratios for the cases where the curves were flat in the vicinity of the minimum.

A comparison of the optimum temperature ratios T_2/T_1 and T_4/T_1 obtained by this work and by the method of reference 1 based on minimum prime radiating area and fixed heat-transfer coefficient h_R is plotted in figures 8 and 9, respectively, as a function of cycle loss pressure ratio. Both calculations used the same temperature ratio increments and selection process. The specific values of optimum T_2/T_1 and T_4/T_1 for helium, neon, and argon fell within the maximum error band, so that a single curve can be plotted for all three gases. As can be seen from these figures, optimization of temperatures using the radiator model yields slightly higher values of both T_2/T_1 and

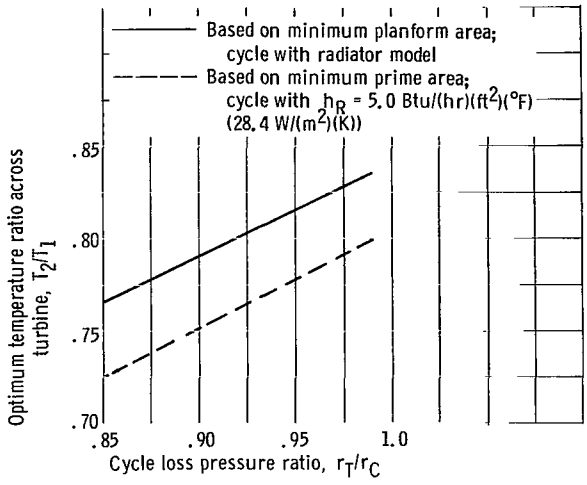

Figure 8. - Variation of optimum temperature ratio across turbine with cycle loss pressure ratio. Average for helium, argon, and neon. Maximum error band, ±0.025 on temperature ratio.

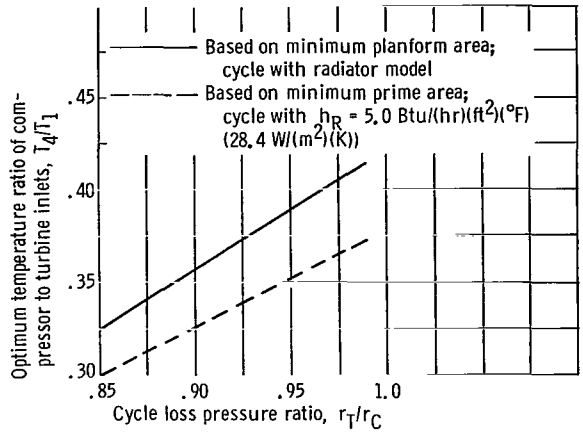

Figure 9. - Variation of optimum temperature ratios of compressor to turbine inlet with cycle loss pressure ratio. Average for helium, argon, and neon. Maximum error band, ±0.025 on temperature ratio.

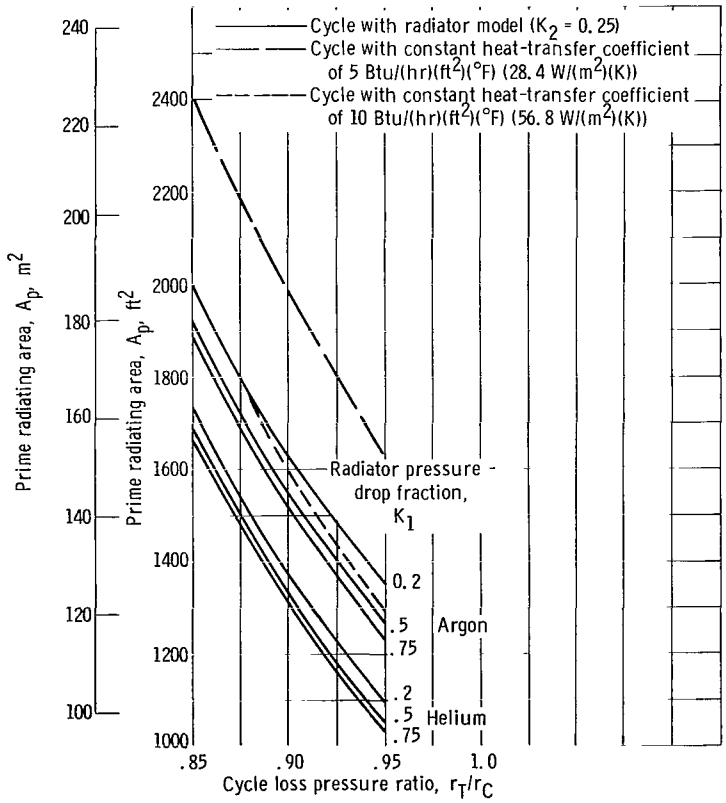

Figure 10. - Variation of prime radiating area with cycle loss pressure ratio at optimum temperature ratios. Gas Reynolds number, 50 000.

T_4/T_1 for all three gases. This is attributed to the difference in the value of h_R used in each method. A further indication of the effect of the value of h_R as computed by the two approaches is shown by figure 10. Figure 10 is a plot of prime radiating area as a function of cycle loss pressure ratio with K_1 as a parameter for argon and helium, and of prime radiating area obtained by using a constant value of h_R = 5 and 10 Btu per hour per square foot per ^{o}F (28.4 and 56.8 $W/(m^2)(K)$) included as a comparison. The lower values of prime radiating area obtained in this study (for helium and argon) as shown in figure 10 are due to the higher values of the actual heat-transfer coefficient h_R obtained in the analysis compared with the constant values.

The numerical results also indicated that, within the optimization selection process used, neither radiator pressure-drop fraction K_1, nor gas Reynolds number has any effect on the optimum temperature ratios for a given gas and cycle loss pressure ratio. However, as shown in figures 9 and 10, the optimum temperature ratios tended to increase with increasing cycle loss pressure ratio for all three gases.

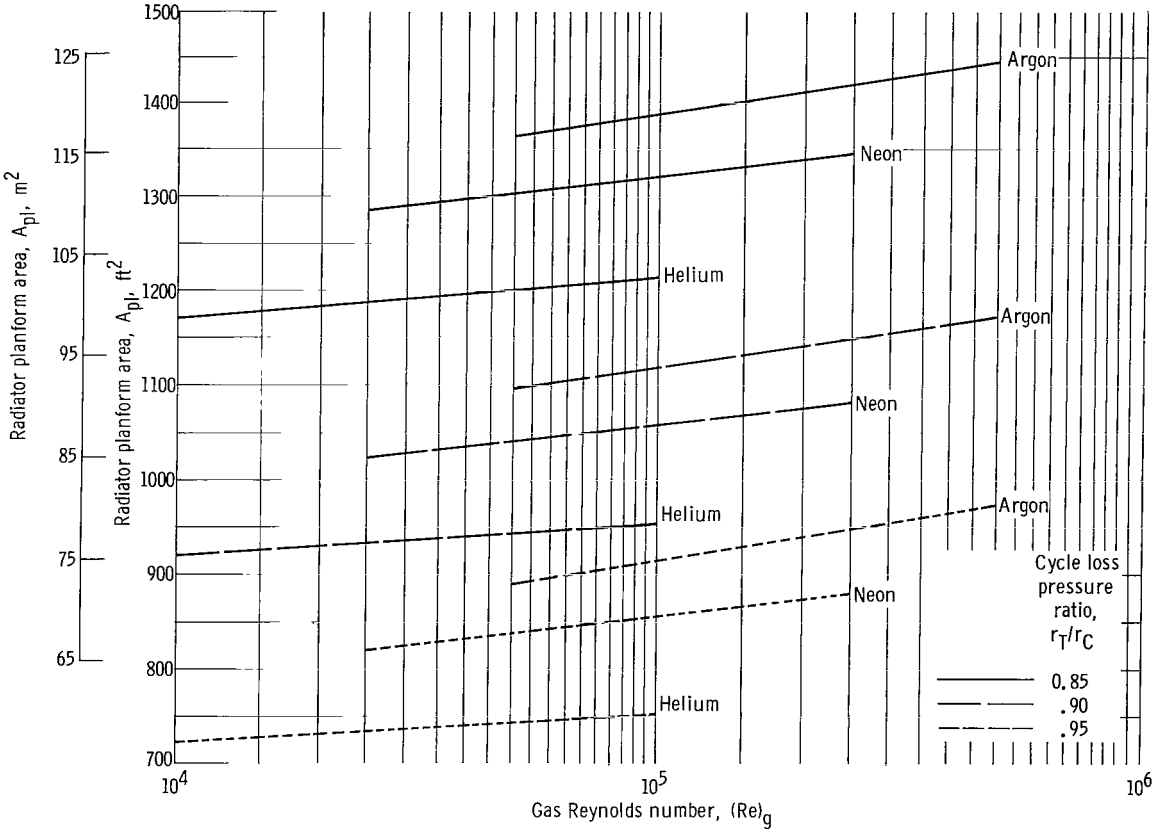

Figure 11. - Variation of radiator planform area with gas Reynolds number. Radiator pressure-drop fraction, 0.5; recuperator pressure-drop fraction, 0.25.

In order to present smooth curves for the radiator geometry factors (L, N, D_i, etc.), some of the operating conditions chosen were not exactly at the precise minimum value of the planform area. However, these points were always within ±0.025 of the temperature ratios at the precise minimum A_{pl} and always within 0.5 percent of the value of minimum planform area.

Planform area. - The effect of gas Reynolds number on the radiator planform area at the optimum temperature ratios and fixed radiator pressure-drop fraction K_1 is shown in figure 11. As can be seen from this figure, the effect of gas Reynolds number is to increase the value of A_{pl} monotonically as $(Re)_g$ is increased over the range of interest for each gas and cycle loss pressure ratio considered. The magnitute of this increase, however, is small (only around 5 to 10 percent over the range of Reynolds numbers considered).

The variation of radiator planform area with radiator pressure-drop fraction, K_1, at a fixed Reynolds number of 50 000 is shown in figure 12 for several values of cycle

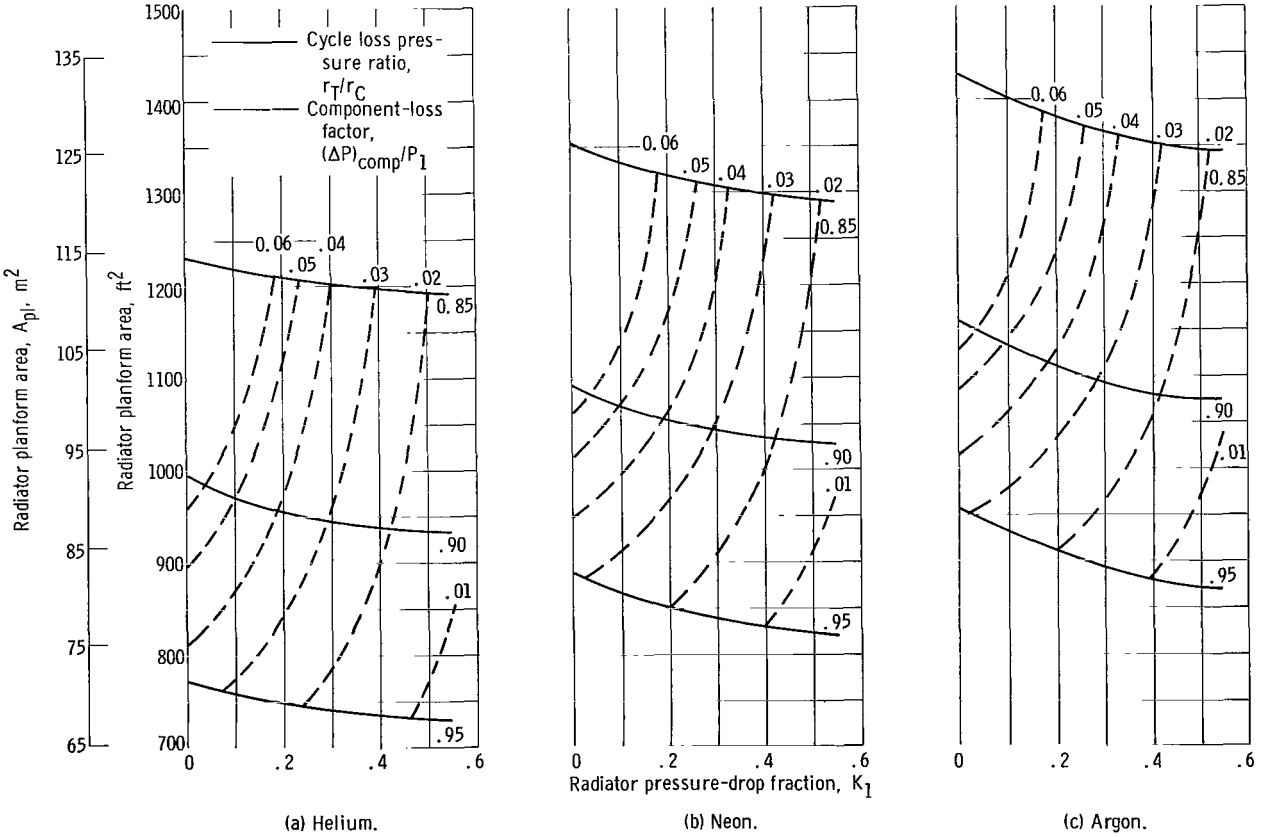

Figure 12. - Variation of radiator planform area with radiator pressure-drop fraction at optimum temperature ratios. Gas Reynolds number, 50 000; recuperator pressure-drop fraction, 0.25.

loss pressure ratio and component-loss factor $((\Delta P)_{comp}/P_1)$ for helium, neon and argon respectively. The figure indicates that an increase in K_1 from 0.2 to 0.75 at constant cycle loss pressure ratio does not affect the planform area appreciably (less than a 10 percent decrease in A_{pl} for the range of K_1 covered). However, if a fixed component loss is prescribed, a substantial reduction in planform area results from reductions in K_1 because of the effect on r_T/r_C. Thus, the planform area is much more sensitive to the value of overall cycle loss pressure ratio than to the value of K_1.

Tube geometry. - The variation of tube length with gas Reynolds number at optimum temperature ratio conditions and fixed K_1 is shown in figure 13 for three gases and

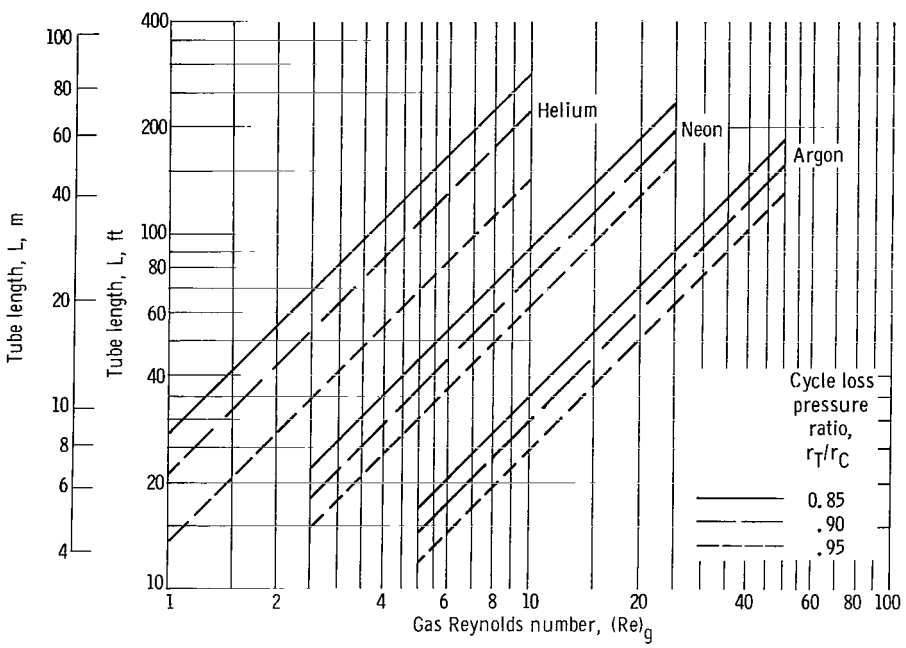

Figure 13. - Variation of tube length with gas Reynolds number. Radiator pressure-drop fraction, 0.5; recuperator pressure-drop fraction, 0.25.

cycle loss pressure ratios. The figure shows that L varies linearly with $(Re)_g$, as indicated by equation (25). It appears that the use of helium results in much longer tubes than the use of argon or neon for the same conditions. The effect of the cycle loss pressure ratio appears to depend on the gas used; the effect being largest with helium. In all cases the tube length decreases with increasing cycle loss pressure ratio.

The effect of radiator pressure-drop fraction K_1 on the tube length was relatively minor (less than 10-percent decrease in length for an increase of K_1 from 0.2 to 0.75 compared with the effect of the other factors involved over the range of variables covered.

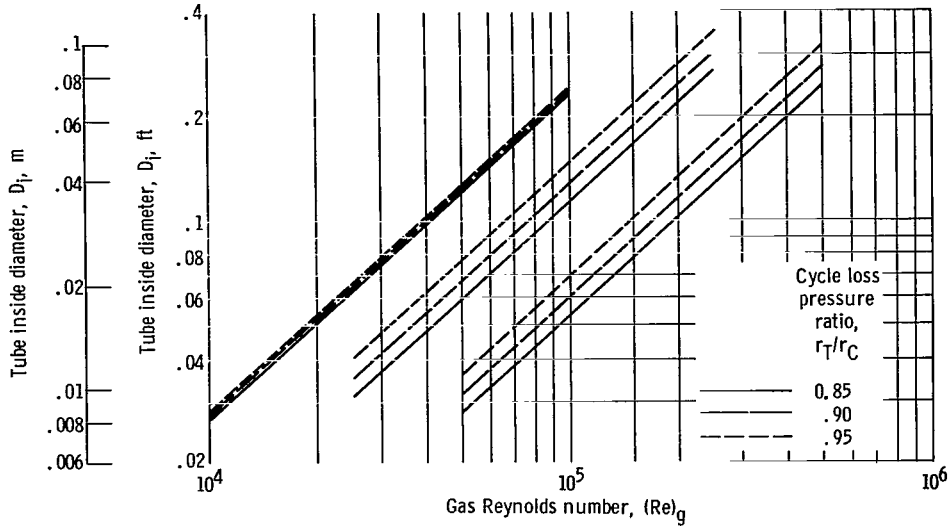

Figure 14. - Variation of tube inside diameter with gas Reynolds number. Radiator pressure-drop fraction, 0.5; recuperator pressure-drop fraction, 0.25.

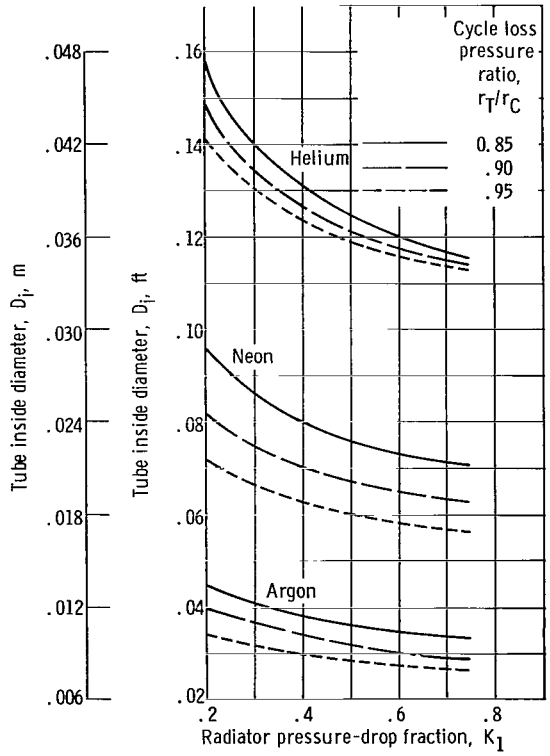

Figure 15. - Variation of tube inside diameter with radiator pressure-drop fraction. Gas Reynolds number, 50 000; recuperator pressure-drop fraction, 0.25.

The gas Reynolds number also has a very strong effect on the tube inside diameter, as illustrated in figure 14. The linear dependency of D_i on Reynolds number can be seen from equation (24) because L varies linearly with Reynolds number. The figure also indicates the large effect that the gas exerts on the tube diameter; the tube diameters needed with helium as the working fluid are almost four times those required using argon as the working fluid for the same Reynolds number and cycle loss pressure ratio.

The effect of the radiator pressure-drop fraction K_1 on the tube inside diameter is shown in figure 15, with r_T/r_C as a parameter at a constant $(Re)_g$ of 50 000. As K_1 decreases (corresponding to decreasing values of the pressure drop across the radiator) the tube diameters become larger as would be expected for a lower pressure drop. The effect of the cycle loss pressure ratio, appears generally small in comparison with the effects of Reynolds number and gas used.

Equation (27) shows that the number of tubes is inversely proportional to the square of the tube diameter. Because the tube diameter is almost linear with Reynolds number, N will vary approximately with the inverse square of the Reynolds number. Because either decreasing r_T/r_C or increasing K_1 results in a higher pressure drop across the radiator (see fig. 3), the number of tubes will tend to increase with a decrease in

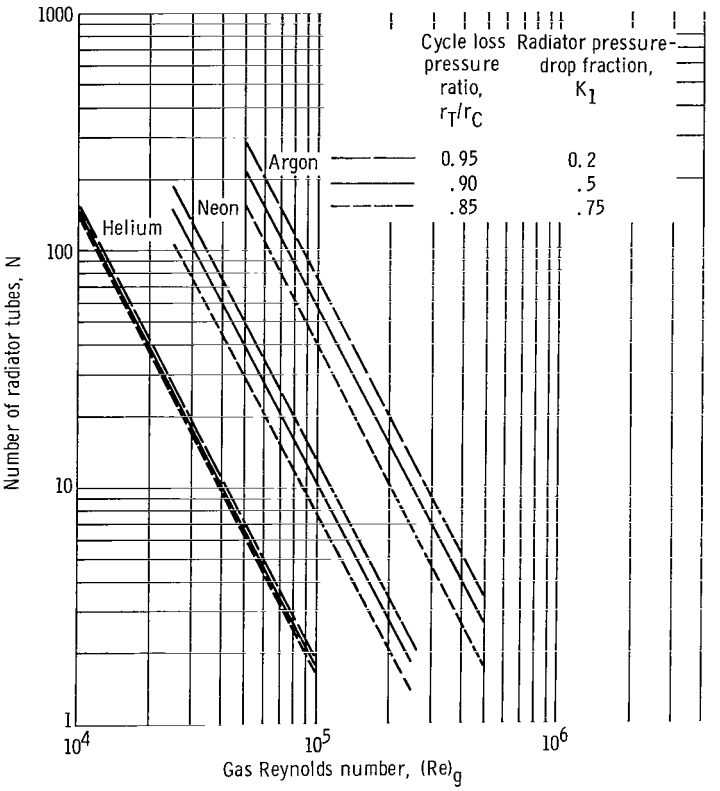

Figure 16. - Variation of number of radiator tubes with gas Reynolds number. Recuperator pressure-drop fraction, 0.25.

r_T/r_C or an increase in K_1. However, the variation of N with r_T/r_C and K_1 was relatively small. Figure 16 illustrates the effect of a combination of these two variables that results in the maximum variation in the number of tubes. It is thus seen that the two major factors affecting the tube geometry (L, D_i, and N) are the gas used and the gas flow Reynolds number.

Heat-transfer coefficient. - The major factors which influence the heat-transfer coefficient based on radiating area h_R appear to be the gas used, the radiator pressure-drop fraction K_1, and the gas Reynolds number. Plots of h_R against $(Re)_g$ for helium, neon, and argon, are shown in figure 17 for a fixed value of r_T/r_C. Al-

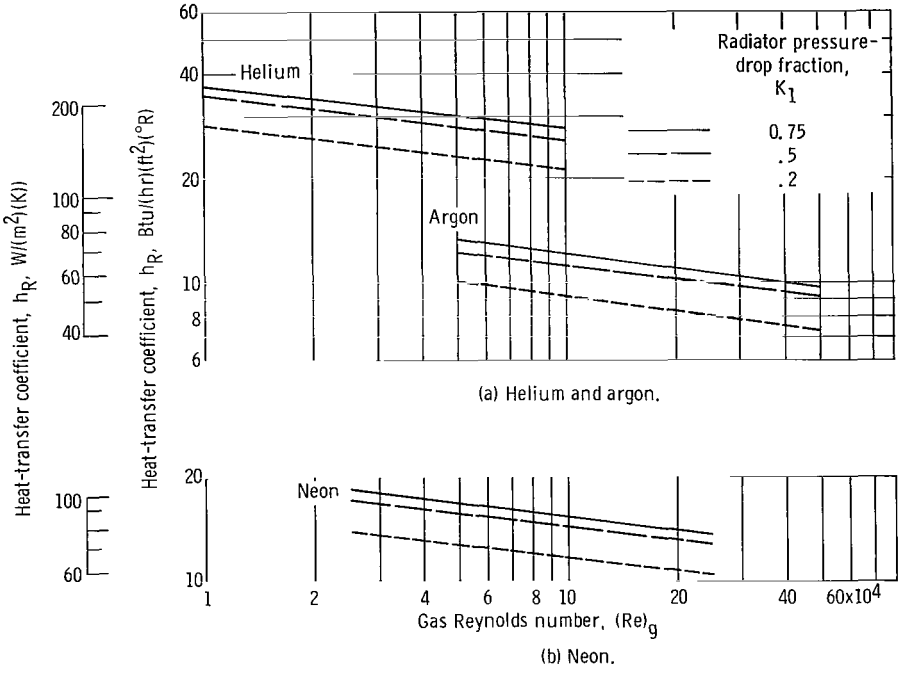

Figure 17. - Variation of heat-transfer coefficient with gas Reynolds number. Cycle loss pressure ratio, 0.90; recuperator pressure-drop fraction, 0.25.

though h_R is proportional to $(Re)_g^{0.8}$, it is also inversely proportional to D_i, which increases with increasing $(Re)_g$ (see fig. 14). The net effect is that h_R decreases with $(Re)_g$ as indicated in the figure. The fact that higher values of K_1 resulted in higher heat-transfer coefficients was expected because a high value of K_1 represents a large allowable pressure drop through the radiator tubes and hence results in a small tube diameter. Similar trends of variation of h_R were obtained at the other values of the cycle loss pressure ratio.

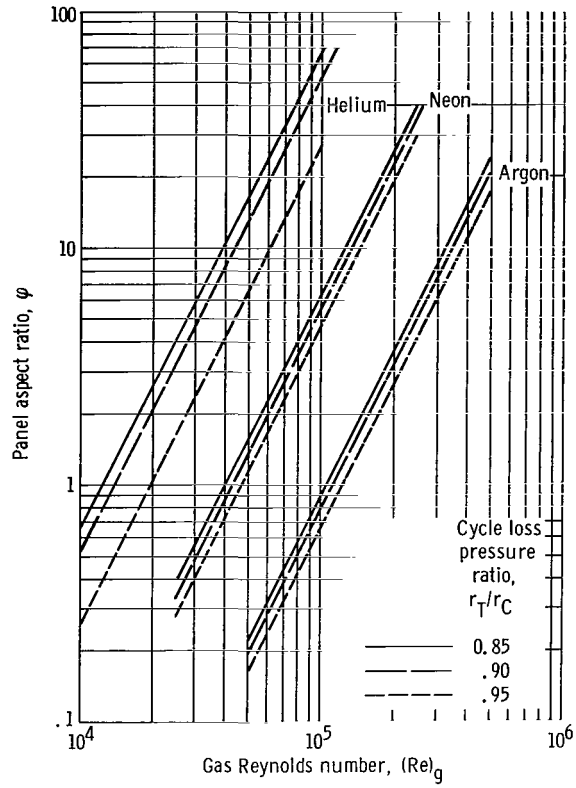

Figure 18. - Variation of panel aspect ratio with gas Reynolds number. Radiator pressure-drop fraction, 0.5. Recuperator pressure-drop fraction, 0.25.

Panel aspect ratio. - Figure 18 shows the variation of the panel aspect ratio (eq. (31)) against gas Reynolds number with the cycle loss pressure ratio at a fixed value of K_1. If radiator design considerations limit the aspect ratio over a certain range (e.g., 0.5 to 2) then these curves indicate the appropriate Reynolds number range of operation. The figures show that the major influences on the aspect ratio are the gas used and the Reynolds number. At a given Reynolds number, the use of helium results in a panel aspect ratio approximately 10 times that of neon and 100 times that of argon. Increasing the cycle loss pressure ratio (at constant $(Re)_g$) decreases the aspect ratio as indicated in the figures, whereas varying K_1 had a negligible effect on the aspect ratio (less than 10 percent for a change in K_1 from 0.2 to 0.75). Thus, even at low radiator pressure drops (high r_T/r_C and low K_1), reasonable panel aspect ratios (0.5 to 2) are obtainable for all three bases if the Reynolds number is appropriately chosen.

Gas velocity. - The effect of gas Reynolds number and radiator pressure-drop fraction on the average and inlet velocity through the tubes is illustrated in figures 19 and 20, respectively. The inlet velocity is approximately 20 percent higher than the

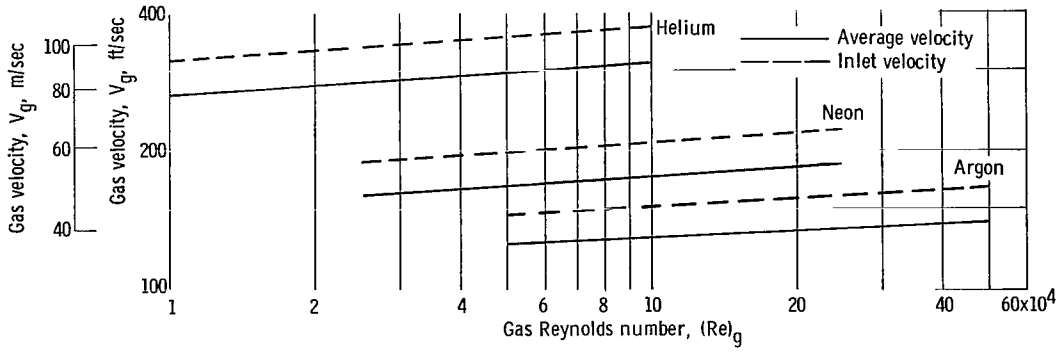

Figure 19. - Variation of velocity of gas in tubes with gas Reynolds number. Cycle loss pressure ratio, 0.90; radiator pressure-drop fraction, 0.5; recuperator pressure-drop fraction, 0.25.

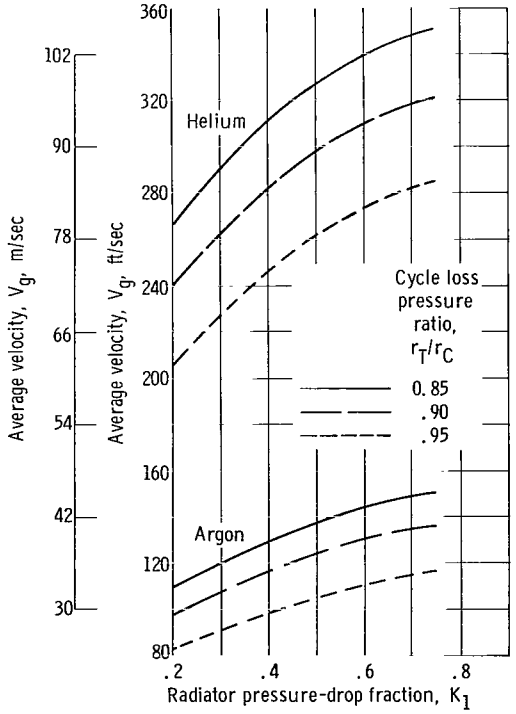

Figure 20. - Variation of average velocity with radiator pressure-drop fraction. Gas Reynolds number, 50 000; recuperator pressure-drop fraction, 0.25.

average velocity. The velocity along the tubes using helium is more than double that using argon, all other factors being equal. Figure 19 shows that the velocity increases slightly with Reynolds number. Figure 20, shows that a decrease in K_1 from 0.75 to 0.2 results in a decrease in the average velocity because the allowable pressure drop in the tubes is reduced; whereas, an increase in r_T/r_C from 0.85 to 0.95 causes a decrease in velocity for similar reasons. Because all the velocities computed were substantially below the acoustic velocity, the assumption of incompressible flow used in the analysis is acceptable.

Gas-Solid Suspension Results

The effect on radiator characteristics of the use of a gas-solid suspension as the cycle working fluid was determined for three suspensions: graphite-helium, graphite-neon, and graphite-argon. Inasmuch as the primary emphasis in these calculations was on the effect of the particle loading ratio of the suspension and since previous results indicated that the effects of r_T/r_C and K_1 were generally smaller than those of the gas used and the gas-flow Reynolds number, the calculations were conducted for a single value of cycle loss pressure ratio of 0.90 and radiator pressure-drop fraction of 0.5. The minimum value of the planform area was selected as the criterion for determining both the optimum cycle temperature ratios and the optimum particle loading ratio for each gas. As indicated previously, property data for the suspensions were obtained from the correlations of reference 5.

Optimum temperature ratios. - Plots of optimum T_2/T_1 and T_4/T_1 against particle loading ratios are shown in figures 21 and 22. As can be seen in the figures, both

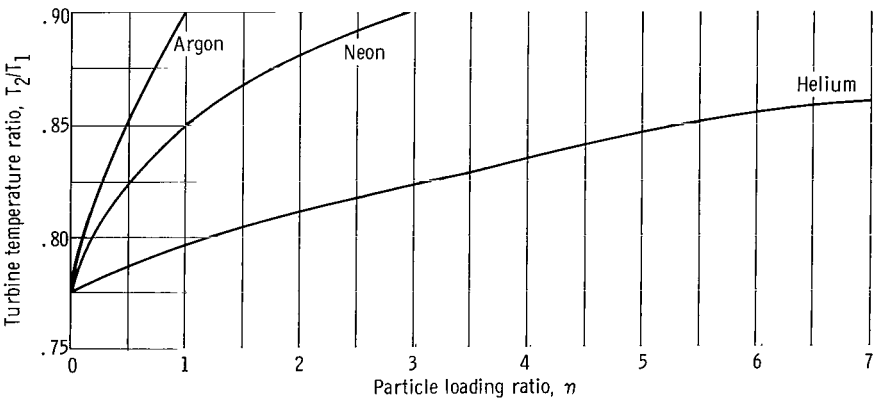

Figure 21. - Variation of optimum temperature ratio with particle loading ratio. Cycle loss pressure ratio, 0.90; radiator pressure-drop fraction, 0.5; recuperator pressure-drop fraction, 0.25.

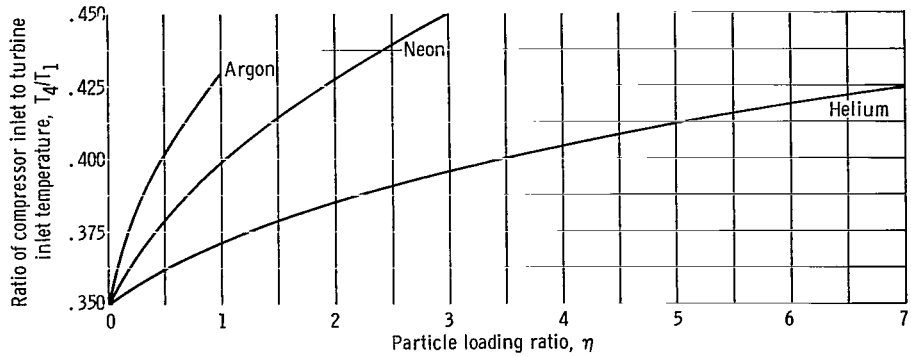

Figure 22. - Variation of optimum ratio of compressor inlet to turbine inlet temperature with particle loading ratio. Cycle loss pressure ratio, 0.90; radiator pressure-drop fraction, 0.5; recuperator pressure-drop fraction, 0.25.

of the optimum temperature ratios increase with increasing particle concentration. The rate of increase is smallest with helium and most pronounced with argon. The increase in the optimum temperature ratios with increasing particle loading ratio is due to the fact that the isentropic specific-heat ratio γ_s decreases with particle loading ratio. Therefore, the temperature difference across both the turbine and compressor decrease. The disparity in the optimum temperature ratios for the three different suspension carrier gases is due to the difference in the specific heat of the gases resulting in different values of δ for each suspension.

Planform area. - The variation of panel planform area with particle loading ratio at several gas Reynolds numbers for three gas-graphite suspensions is plotted in figure 23. Values of the planform area for $\eta = 0$ represent the pure-gas case.

The figures show that a minimum planform area is obtained at a specific particle loading ratio for each gas, and this optimum particle loading ratio varies only slightly with the gas Reynolds number. For the helium suspension, the optimum particle loading ratio is between 4.5 and 6.0 for the range of Reynolds numbers covered. For the neon suspension, the optimum particle loading ratio is around 0.75 and 1.0, and, for the argon suspension, the optimum particle loading ratio falls between 0.30 and 0.40 for the respective ranges of representative gas Reynolds number. A plot of optimum particle loading ratio against Reynolds number is shown in figure 24 for all three gases.

A minimum of the planform area with increasing particle loading ratio occurs because of the opposing effects of the isentropic specific-heat ratio and the convective heat-transfer coefficient h_R. For a given gas, an increase in the particle loading ratio decreases γ_s, increases the cycle efficiency, and thus tends to decrease the planform area. At the same time, an increase in η decreases h_R (as will be subsequently explained) and, therefore, tends to increase the planform area.

Because γ_s and h_R are both functions only of the product of the particle loading

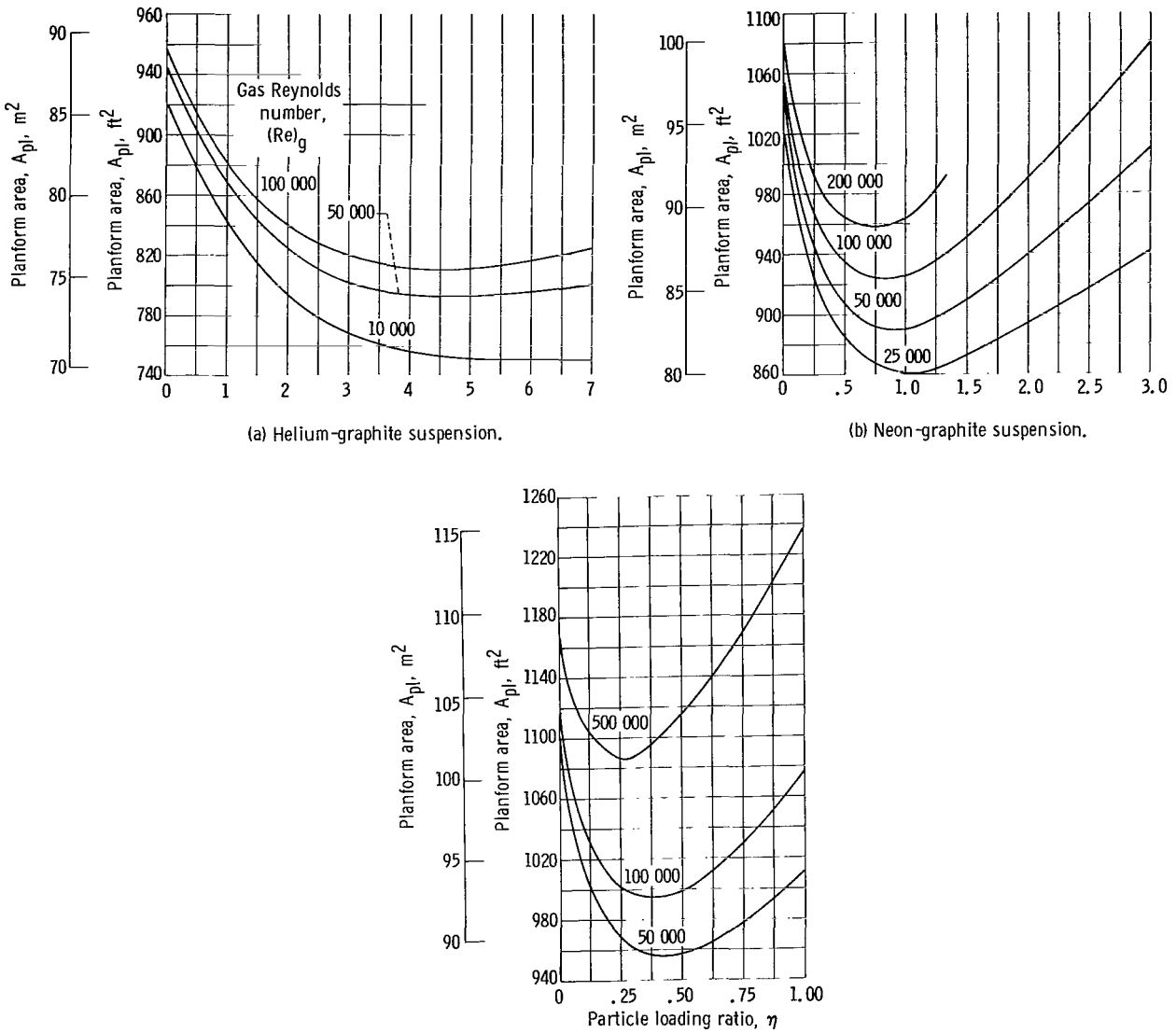

(a) Helium-graphite suspension.

(b) Neon-graphite suspension.

(c) Argon-graphite suspension.

Figure 23. - Variation of planform area with particle loading ratio for different gas Reynolds numbers. Cycle loss pressure ratio, 0.90; radiator pressure-drop fraction, 0.5; recuperator pressure-drop fraction, 0.25.

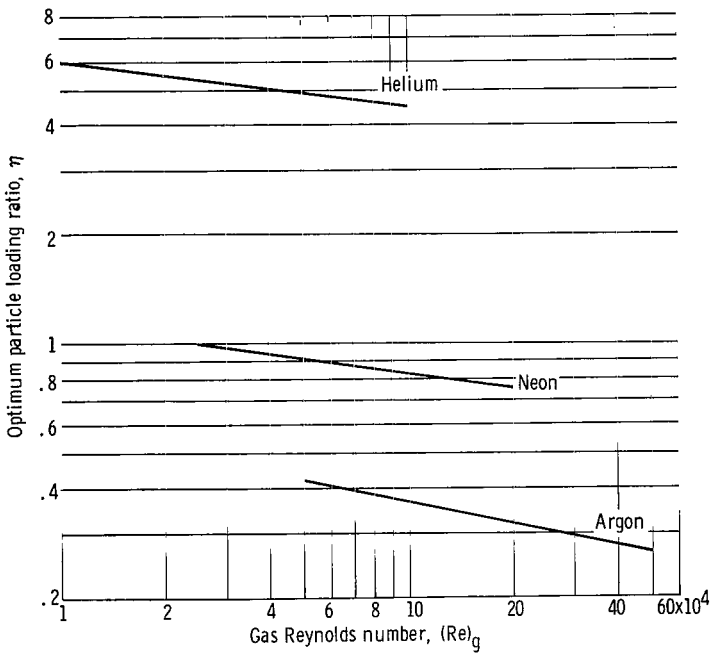

Figure 24. - Variation of optimum particle loading ratio with gas Reynolds number. Cycle loss pressure ratio, 0.90; radiator pressure-drop fraction, 0.5; recuperator pressure-drop fraction, 0.25.

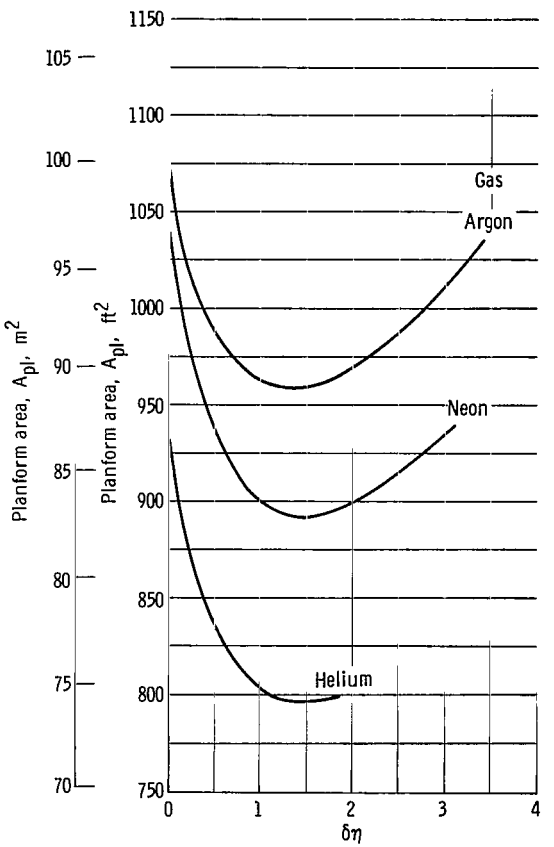

Figure 25. - Variation of planform area with product $\delta\eta$. Gas Reynolds number, 50 000; cycle loss pressure ratio, 0.90; radiator pressure-drop fraction, 0.5; recuperator pressure-drop fraction, 0.25.

ratio times the ratio of the heat capacities of the solid to the gas $\delta\eta$, it is the value of this quantity which determines the minimum planform area. This is illustrated in figure 25, which shows that, at a gas Reynolds number of 50 000 for all three graphite-gas suspensions considered, the minimum planform area occurs at approximately the same value of $\delta\eta$ equal to 1.4.

The magnitude of the maximum decrease in panel planform area potentially achievable with the use of a gas-solid suspension is more graphically illustrated in the plots of the ratio of planform area of the suspension to that of the pure gas $A_{pl}(\eta = opt)/A_{pl}(\eta = 0)$ (fig. 26). Compared with the pure-gas, average reductions in panel planform area from 17 percent for helium to 10 percent for argon are indicated for the range of variables covered.

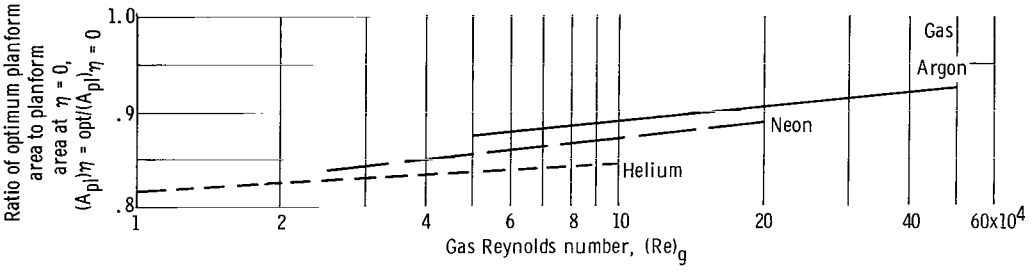

Figure 26. - Variation of ratio of planform area at optimum particle loading ratio to planform area at zero particle loading ratio with gas Reynolds number. Cycle loss pressure ratio, 0.90; radiator pressure-drop fraction, 0.5; recuperator pressure-drop fraction, 0.25.

The empirical friction factor and heat-transfer correlations used in the suspension radiator calculations contained extrapolated values for loading ratios lower than 1.0 as discussed in reference 5. Therefore, there is some uncertainty in the absolute magnitude of the resultant values of radiator geometry and in the optimum values of particle loading ratios as determined herein.

Tube geometry. - The effect of particle loading ratio on tube geometry is illustrated in figures 27 to 29 by plots of the calculated variations of N, D_i, and L at representative optimum particle loading ratio against gas Reynolds number as compared with the corresponding values for the pure-gas case ($\eta = 0$). The results in all cases are for the optimum values of T_2/T_1 and T_4/T_1 for each suspension system. It is seen from figure 27, that the use of an optimum particle loading ratio markedly reduces the required number of tubes at a given Reynolds number. The ratio between the suspension and pure-gas cases averages between 0.25 and 0.36 for the range of conditions covered.

Figure 28 shows an increase in tube length with the use of an optimum loading ratio. The average ratio of suspension length to pure-gas length varied from around 1.55 to 1.75. The suspension also results in an increase in tube inside diameter for a given gas

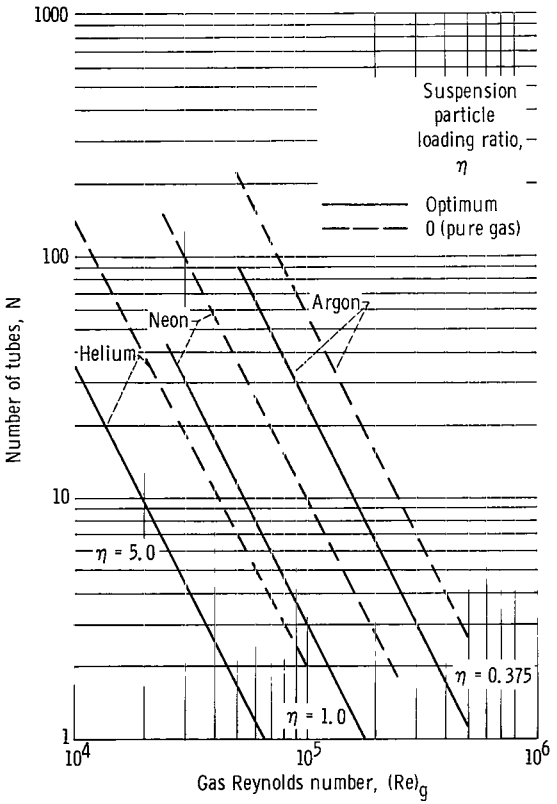

Figure 27. - Variation of number of radiator tubes with gas Reynolds numbers at representative particle loading ratios. Cycle loss pressure ratio, 0.90; radiator pressure-drop fraction, 0.5; recuperator pressure-drop fraction, 0.25.

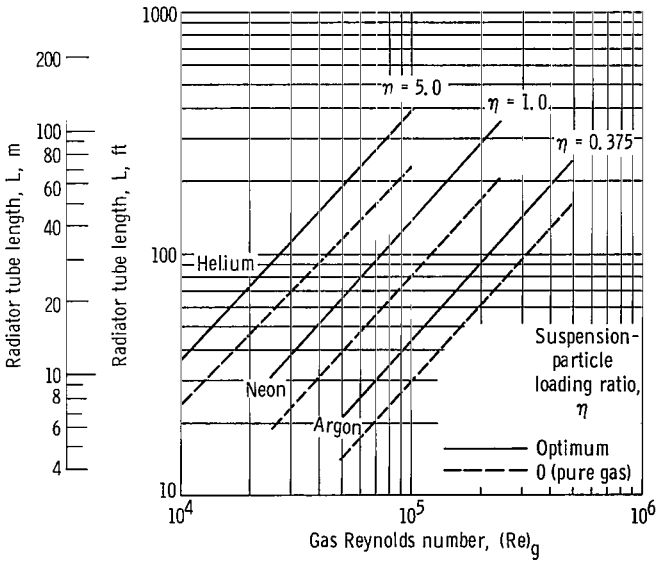

Figure 28. - Variation of radiator tube length with gas Reynolds number at representative particle loading ratios. Cycle loss pressure ratio, 0.90; radiator pressure-drop fraction, 0.5; recuperator pressure-drop fraction, 0.25.

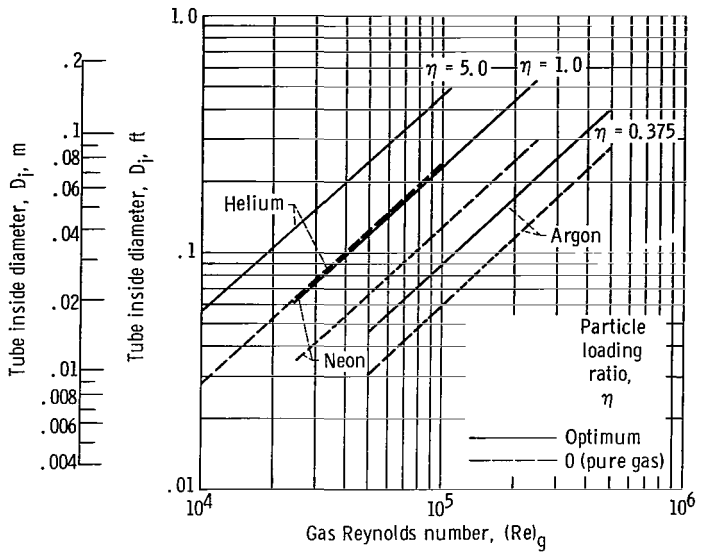

Figure 29. - Variation of radiator tube inside diameter with gas Reynolds number at representative particle loading ratios. Cycle loss pressure ratio, 0.90; radiator pressure-drop fraction, 0.5; recuperator pressure-drop fraction, 0.25.

Reynolds number (fig. 29). The ratios in this case also varied somewhat with the gas used: around 1.95 for helium, 1.60 for argon, and 1.75 for neon.

Panel aspect ratio. - The panel aspect ratio is also greater at a given Reynolds number with the use of a gas-solid suspension (see fig. 30). Average ratios vary from around 2.7 for argon to 3.5 for neon. The increase in panel aspect ratio is primarily the result of the reduction in number of tubes and increase in tube length as indicated in figures 28 and 29. If the radiator panel aspect ratio is restricted to a certain range of values because of the specific application of the radiator, figure 12 can be used to determine the approximate Reynolds number range of operation. For example, if the panel aspect ratio is required to be 2.0, the operating gas Reynolds number should be around 11 000 for helium-graphite, 33 000 for neon-graphite, and 105 000 for argon-graphite suspensions at optimum conditions.

Heat-transfer coefficient. - The effect of the gas-solid suspension on the heat-transfer coefficient based on radiator area h_R is illustrated in figure 31. The values of h_R for the suspension are lower than for the pure gas. This apparent anomoly is due to the relative variations of h_i for the pure gas and for the suspension. Although, the ratio h_s/h_g increases for a given tube diameter as loading ratio is increased (as indicated by eq. (16)), for the optimum loading ratios considered, the tube diameter is greater than for the pure-gas case at a given Reynolds number (fig. 29). Thus, there is a net decrease in the value of h_s compared with h_g at a given gas flow Reynolds

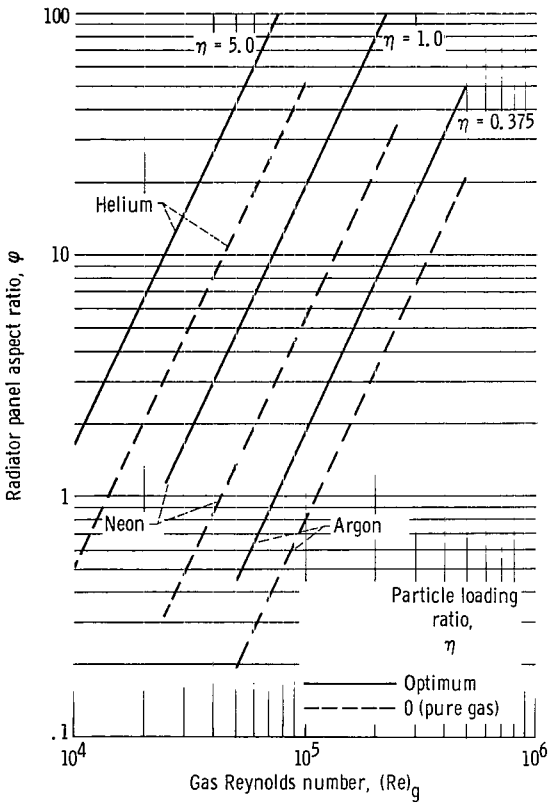

Figure 30. - Variation of panel aspect ratio with Reynolds number for representative particle loading ratios. Cycle loss pressure ratio, 0.90; radiator pressure-drop fraction, 0.5; recuperator pressure-drop fraction, 0.25.

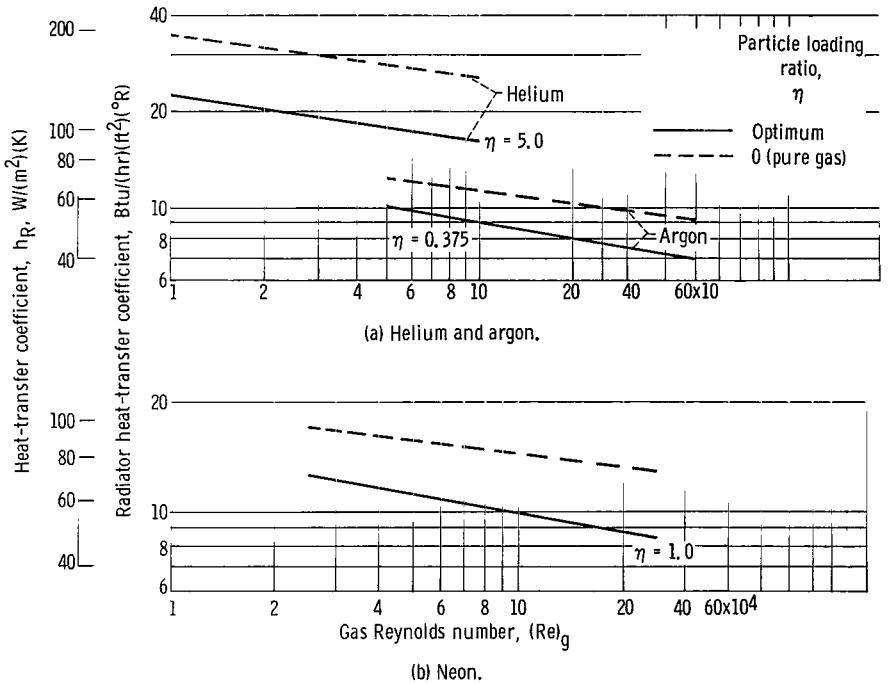

Figure 31. - Variation of radiator heat-transfer coefficient with Reynolds number at representative particle loading ratios. Cycle loss pressure ratio, 0.90; radiator pressure-drop fraction, 0.5; recuperator pressure-drop fraction, 0.25.

number, and, with A_i/A_p a constant in all cases (eq. (22)), there is a net reduction in h_R for the suspension compared with the pure-gas case.

Weight comparison. - The results of figure 26 indicated a relatively modest reduction in radiator planform area with the use of a graphite-gas suspension at a representative optimum particle loading ratio. Although the radiator model and computation procedure were not originally devised to investigate radiator weight, it is possible, on the basis of the present analysis, to obtain a comparison of approximate weights of pure-gas and suspension radiators. The development of the weight equations for the radiator fin tube model of figure 4 is detailed in appendix F. From this development, it is shown that the ratio of suspension radiator weight is

$$\frac{W_s}{W_g} = \frac{\left(A_{pl}\right)_s}{\left(A_{pl}\right)_g} \frac{\left(D_i\right)_s}{\left(D_i\right)_g} \frac{\left(\frac{D_o}{D_i}\right)_s}{\left(\frac{D_o}{D_i}\right)_g} \left\{ \frac{\frac{\pi}{4}\left[1 - \left(\frac{D_i}{D_o}\right)_g^2 \frac{\left(\frac{D_o}{D_i}\right)_g^2}{\left(\frac{D_o}{D_i}\right)_s^2}\right] + 2\left(\frac{\rho_f}{\rho_t}\right)_s \left(\frac{l_f}{D_o}\right)_s \left(\frac{t_f}{D_o}\right)_s}{\frac{\pi}{4}\left[1 - \left(\frac{D_i}{D_o}\right)_g^2\right] + 2\left(\frac{\rho_f}{\rho_t}\right)_g \left(\frac{l_f}{D_o}\right)_g \left(\frac{t_f}{D_o}\right)_g} \right\} \tag{32}$$

in which values of A_{pl} and D_i are obtained from the comparable calculated results of the pure-gas and suspension cases (i.e., figs. 11, 23, 26, and 29). Thus, for the prescribed values of $\left(D_o/D_i\right)_g$ and l_f/D_o, and the assumption that ρ_f/ρ_t, l_f/D_o are the same for the pure-gas and suspension cases, ratios of radiator weight can be obtained from equation (32) if the value of $\left(D_o/D_i\right)_s/\left(D_o/D_i\right)_g$ is known or prescribed.

Although D_o/D_i has been specified to be 1.33, for both the pure-gas and suspension, it is likely that this value might be reduced for the case of the suspension because a larger tube inside diameter is obtained at any fixed Reynolds number (fig. 29). Thus, it would be of interest to plot the variation of weight ratio W_s/W_g as a function of the ratio $\left(D_o/D_i\right)_s/\left(D_o/D_i\right)_g$ for several representative values of fin thickness parameter t_f/D_o. Calculations of these variations for the three gases were made for $\left(D_o/D_i\right)_g = 1.33$, $l_f/D_o = 3.5$, $\rho_f/\rho_t = 1.0$ and 3.4, and $t_f/D_o = 0.02$ and 0.04. Com-

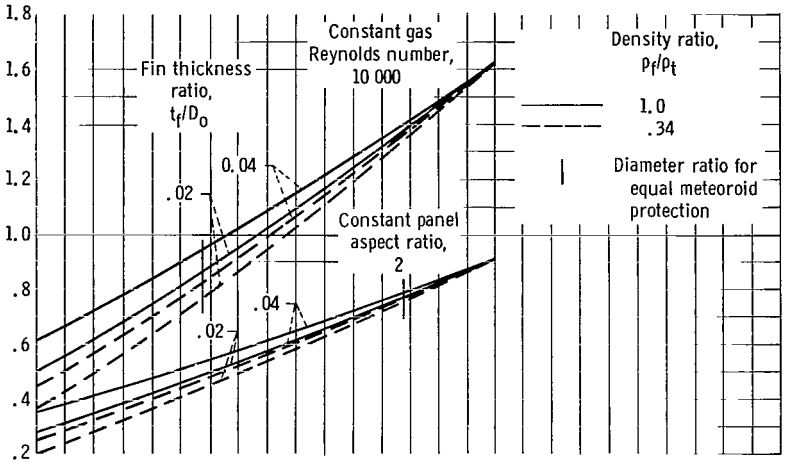

(a) Helium; optimum suspension-particle loading ratio, 5.

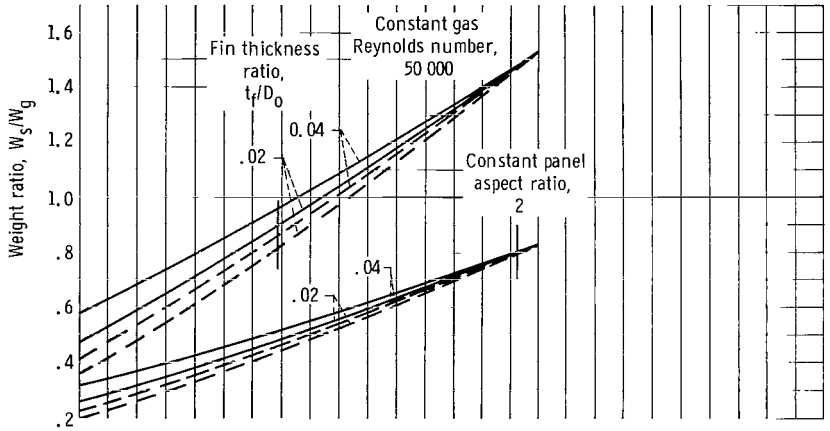

(b) Neon; optimum suspension-particle loading ratio, 1.

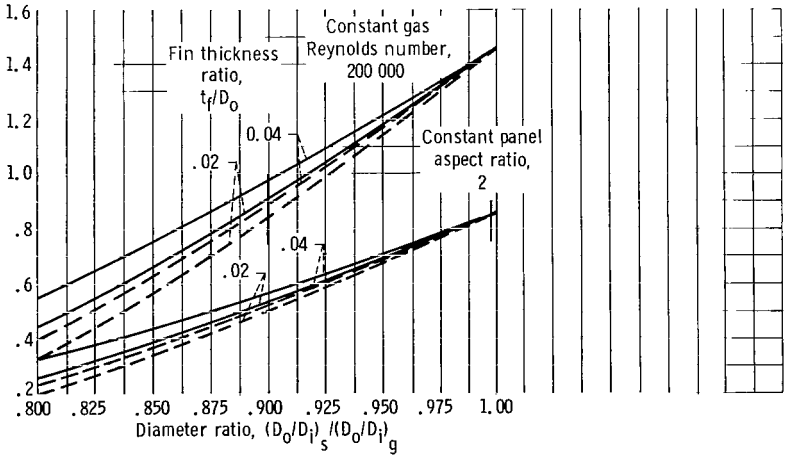

(c) Argon; optimum suspension-particle loading ratio, 0.375.

Figure 32. - Variation of radiator weight ratio with outside-to-inside tube diameter ratio. Gas outside-to-inside tube diameter ratio, 1.33; fin length to tube outside diameter ratio, 3.5; fin length to tube outside diameter ratio, fin thickness to tube outside diameter ratio, and fin to tube density ratio are same for gas and suspension.

parisons were then made on the basis of the same gas Reynolds number for the pure-gas and suspension cases, and also on the basis of the same panel aspect ratio for the pure-gas and suspension cases, as shown in figure 32. Also shown in the figure are the values of tube diameter ratio for the criterion of equal meteoroid protection for the pure-gas and suspension cases. These values represent likely or realistic values of suspension tube diameter ratio $\left(D_o/D_i\right)_s$ as obtained from consideration of meteoroid protection theory in determining tube wall thickness (appendix F).

Figure 32 shows that a substantial reduction in radiator weight is possible with the use of a suspension working fluid if the tube wall thickness can be decreased to give reduced values of $\left(D_o/D_i\right)_s$. For the practical case of tube wall thickness required for equal meteoroid protection, it appears that the weight reduction for the suspension radiators for constant aspect ratios is somewhat greater than for the constant Reynolds number. For the fixed Reynolds number cases, the weight reduction varied from around 2 to 20 percent (while the planform area reduction (fig. 26) varied from around 10 to 18 percent). For a panel aspect ratio of 2.0, the weight reduction for the suspension radiators compared with the pure-gas radiators was around 15 to 25 percent (comparable planform area reduction is 12 to 19 percent). For both comparison bases, helium showed the largest weight reduction percentage, and argon showed the smallest reduction.

In view of the reduced values of D_o/D_i indicated for the fixed Reynolds-number suspension radiators when compared for equal meteoroid protection (around 1.16 to 1.20 compared with 1.33 for the pure-gas radiator model), check calculations were made to determine the effect of a reduced value of D_o/D_i on the calculated planform area of the suspension radiators. These results indicated an average reduction in suspension radiator planform area of around 2 percent. A more precise determination of planform area and weight reductions for the suspension radiators will require a more exact radiator analysis such as that illustrated by reference 7.

Comparison with results of reference 6. - An analysis of the use of a suspension of graphite particles in argon, neon, and helium as the working fluid in a Brayton space power cycle was also conducted in reference 6. The analysis of reference 6 determined prime radiating area. For the cycle and assumptions considered, the analysis showed first that the prime radiating area decreased rapidly as the product $\delta\eta$ was increased to about 3.0 and then decreased much more slowly with $\delta\eta$. The results obtained in this report indicated that, at a Reynolds number of 50 000, the planform area showed a minimun at a $\delta\eta$ of 1.4. The second result from reference 6 was an indicated reduction in prime radiating area (at $\delta\eta = 3.0$) of around 67 percent compared with the pure-gas cases. Inasmuch as the current analysis revealed only a 10 to 18 percent reduction in planform area at optimum $\delta\eta$, it is important to explore the basis for the differences.

The analysis of reference 6 was based on the equations for cycle efficiency and prime radiating area developed in reference 1 and presented in appendix B. Equilibrium conditions were assumed to exist in all cycle components, and the isentropic specific-heat ratio of the suspension was the same as equation (5). However, the suspension heat-transfer coefficient h_R used in the equation for prime radiating area was taken to vary linearly with $\delta\eta$, according to

$$\left(h_R\right)_s = \delta\eta\left(h_R\right)_g \tag{33}$$

For the analysis of this report, in contrast, it was found that the radiator heat-transfer coefficient h_R, based on the suspension data correlations of reference 5, actually decrease with particle loading ratio (fig. 31) because of the increase in tube inside diameter (eq. (17)). Thus, lower values of prime radiating area showing no minimum with loading ratio can be expected from the analysis of reference 6.

A second difference between the two cycle analyses is the use, in reference 6, of a recuperator scheme in which two zero-gravity gas-solid separators were used. One was located at the outlet of the turbine to bypass the hot particles directly to the inlet of the heat source. The second separator was located at the outlet of the compressor to bypass the cooled particles back to the radiator. Thus, the particle heat recovery occurred at 100-percent efficiency. Inasmuch as the particles constitute a large fraction of the mass of the working fluid, the overall effectiveness of the recuperator is increased. In using this scheme, the overall recuperator effectiveness with the suspension becomes

$$E_s = \frac{E + \delta\eta}{1 + \delta\eta} \tag{34}$$

where E is the normal recuperator effectiveness. Thus, the overall recuperator effectiveness increases asymptotically toward one as the product of $\delta\eta$ is increased.

In order to determine the effect on radiating area of the increased recuperator effectiveness resulting from the use of the particle separator scheme, a set of calculations were performed with the combined radiator and cycle analysis developed in this report, and with the recuperator effectiveness E_s defined by equation (34). Results for a helium-graphite suspension at a particle loading ratio of 7 and a gas Reynolds number of 10 000 showed a decrease in planform area of around 32 percent over the pure-gas case compared with the 18-percent decrease obtained without particle separators. Thus, a large portion of the approximately 67-percent reduction in prime radiating area quoted in reference 6 is probably due to the higher values of h_R produced by the use of equation (33). It appears, therefore, that an accurate evaluation of the relative effec-

tiveness of the use of a gas-solid suspension working fluid will require an accurate radiator analysis method as well as accurate property data for particle suspensions in the loading-ratio region of interest.

SUMMARY OF RESULTS

An exploratory comparative analysis of radiator characteristics for a 100-kilowatt single-loop Brayton space power cycle has been conducted based on a simplified radiator model in which either a pure gas or a graphite-gas suspension was used as the working fluid. Results of the calculations for pure helium, neon, and argon at optimum cycle temperature ratios showed principally that:

1. The radiator planform area was determined primarily by the magnitude of the overall cycle loss pressure ratio and the type of gas used. The fractional pressure drop across the radiator had a significant effect on radiator planform area only if the overall cycle loss pressure ratio was varied as well. For a given value of overall cycle loss pressure ratio, the radiator flow Reynolds number and fractional pressure drop had relatively small influence on the radiator planform area.

2. The radiator gas-flow Reynolds number had a pronounced effect on the radiator geometric characteristics of panel aspect ratio and tube inside diamter, number, and length. For a given Reynolds number, the values of the geometric characteristics varied substantially among the three gases considered. For a fixed panel aspect ratio, the required flow Reynolds number was greatest for argon and least for helium.

For the graphite-gas suspension radiators, principal results indicated that:

3. An optimum particle loading ratio corresponding to minimum planform area was found which varied with the gas used and the flow Reynolds number. Values of optimum cycle temperature ratios at these conditions were greater than for the pure-gas case.

4. Moderate reductions in planform area compared with the pure-gas case were obtained, with an average reduction of 17 percent for helium, 13.5 percent for neon, and 10.5 percent for argon over the range of conditions covered in the analysis.

5. An approximate weight evaluation showed somewhat larger percentage reductions with the use of a graphite suspension, depending on the basis of comparison employed (e.g., fixed Reynolds number, fixed panel aspect ratio, etc.). For a design panel aspect ratio of 2.0, weight reductions of around 22 percent for helium, 20 percent for neon, and 15 percent for argon were indicated for the condition of equal meteoroid protection.

Inasmuch as the results of this exploratory analysis depend on the accuracy of the correlations for the pertinent properties of the gas-solid suspension and also of the geometric properties of the radiator model, a more precise comparative evaluation will require more detailed and sophisticated radiator and cycle analysis methods as well as

more accurate information concerning the properties of particle suspensions at low particle loading ratios in the optimum region. Finally, even if the more precise analysis continues to reveal a significant potential gain in the radiator area and weight with the use of particle suspensions, the ultimate feasibility of such an approach requires consideration of the practical problems involved in the use of such systems.

Lewis Research Center,
National Aeronautics and Space Administration,
Cleveland, Ohio, March 15, 1968,
120-27-04-63-22.

APPENDIX A

SYMBOLS

A_i	radiator tube inside surface area, ft^2; m^2
A_p	prime radiating area, ft^2; m^2
A_{pl}	radiator planform area, ft^2; m^2
A_R	total radiator outside surface area, ft^2; m^2
A_v	radiator vulnerable area, ft^2; m^2
C_p	fluid heat capacity, Btu/(lb mass)(^oR); W/(m^2)(K)
D_i	radiator tube inside diameter, ft; m
D_o	radiator tube outside diameter, ft; m
E	recuperator effectiveness; defined by eq. (B2)
F	correction factor for nonisothermal flow in radiator
f	Fanning friction factor
f'_s	friction factor for a gas-solid suspension based on gas density; defined by eq. (C25)
G	mass velocity, lb mass/(sec)(ft^2); kg/(sec)(m^2)
g_c	gravitational constant, (lb mass/lb force) (ft/sec^2); (kg)(m)/(N)(sec^2)
h	convective heat-transfer coefficient, Btu/(ft^2)(^oR)(hr); (W/(m^2)(K)
h_i	heat-transfer coefficient based on tube inside area, Btu/(ft^2)(^oR)(hr); W/(m^2)(K)
h_R	heat-transfer coefficient based on radiator prime area, Btu/(ft^2)(^oR)(hr); W/(m^2)(K)
K_1	radiator pressure-drop fraction: ratio of pressure drop through radiator to total pressure drop in cycle
K_2	recuperator pressure-drop fraction: ratio of pressure drop through recuperator to cycle cold side pressure drop
k	thermal conductivity of gas, Btu/(sec)(^oR)(ft); W/(m)(K)
L	length of radiator tubes, ft; m
l_f	half width of fin, ft; m

N	number of radiator tubes
P	gas pressure, lb/sq ft; N/m^2
Pr	Prandtl number
P_s	output shaft power, kW
$(\Delta P)_c$	sum of pressure drops across radiator and low pressure side of recuperator (cold-side pressure drop), lb/sq ft; N/m^2
$(\Delta P)_{comp}$	sum of pressure drops of heat-transfer components, excluding radiator, lb/sq ft; N/m^2
$(\Delta P)_h$	sum of pressure drops across heat source and high pressure side of recuperator (hot-side pressure drop), lb/sq ft; N/m^2
$(\Delta P)_{rad}$	pressure drop across radiator, lb/sq ft; N/m^2
$(\Delta P)_{rec}$	pressure drop across cold side of recuperator, lb/sq ft; N/m^2
$(\Delta P)_{tot}$	total pressure drop through heat-transfer components in the cycle, lb/sq ft; N/m^2
Q_{rad}	total heat rejected from radiator
R'	gas constant, (lb force)(ft)/(lb mass)(^oR); J/(kg)(K)
Re	Reynolds number
r_T/r_C	cycle loss pressure ratio, $P_1/P_2/P_5/P_4$
T	absolute temperature, ^oR; K
T_s	equivalent sink temperature, ^oR; K
T_w	absolute temperature of tube outer wall, ^oR; K
t_f	thickness of fin, ft; m
t_t	thickness of radiator tube, ft; m
V	velocity through radiator tubes, ft/sec; m/sec
W	radiator weight, lb mass; kg
w	mass flow rate, lb mass/sec; kg/sec
γ	isentropic specific-heat ratio
δ	ratio of particle to gas specific heats
ϵ	emissivity of radiator tubes and fins
η	loading ratio of suspension, mass flow rate of solids/mass flow rate of gas

η_C	compressor efficiency
η_{cy}	thermodynamic cycle efficiency
η_f	fin efficiency
η_T	turbine efficiency
μ	gas viscosity, lb mass/(ft)(sec); N/(sec)(m^2)
ρ	density, lb mass/ft^3; kg/m^3
ρ_f	density of fin metal, lb mass/ft^3; kg/m^3
ρ_t	density of tube metal, lb mass/ft^3; kg/m^3
σ	Stefan-Boltzman constant, Btu/(ft^2)($^oR^4$); J/(m^2)(K^4)
φ	radiator panel aspect ratio, ratio of overall length to width

Subscripts:

av	average conditions
g	gas
p	particles
s	suspension
1	turbine inlet
2	turbine outlet
3	radiator inlet
4	radiator outlet
5	compressor outlet
6	heat-source inlet

APPENDIX B

CYCLE THERMODYNAMIC RELATIONS

The thermodynamic relations associated with the Brayton cycle are developed in reference 1. The developed relations which are pertinent to the present work are presented as follows:

$$\eta_{cy} = \frac{1 - \frac{T_2}{T_1} - \frac{T_4}{T_1}\left(\frac{1}{\eta_C}\right)\left[\frac{\left(\frac{r_T}{r_C}\right)^{1-\gamma/\gamma}}{1 - \frac{1}{\eta_T}\left(1 - \frac{T_2}{T_1}\right)} - 1\right]}{1 - E\left(\frac{T_2}{T_1}\right) - (1 - E)\frac{T_4}{T_1}\left\{1 + \frac{1}{\eta_c}\left[\frac{\left(\frac{r_T}{r_C}\right)^{1-\gamma/\gamma}}{1 - \frac{1}{\eta_T}\left(1 - \frac{T_2}{T_1}\right)} - 1\right]\right\}} \tag{B1}$$

where the recuperator effectiveness E is given by

$$E = \frac{T_2 - T_3}{T_2 - T_5} = \frac{T_6 - T_5}{T_2 - T_5} \tag{B2}$$

$$\frac{wC_p}{P_s} = \frac{3415}{T_1\left\{1 - \frac{T_2}{T_1} - \frac{T_4}{T_1}\left(\frac{1}{\eta_C}\right)\left[\frac{\left(\frac{r_T}{r_C}\right)^{1-\gamma/\gamma}}{1 - \frac{1}{\eta_T}\left(1 - \frac{T_2}{T_1}\right)} - 1\right]\right\}} \tag{B3}$$

$$\frac{A_p}{P_s} = \frac{wC_p}{P_s}\left\{\frac{1}{h_R}\ln\left(\frac{T_{w,3}^4 - T_s^4}{T_{w,4}^4 - T_s^4}\right) + \frac{1}{4\sigma\epsilon T_s^3}\left[\ln\frac{(T_{w,3} - T_s)(T_{w,4} + T_s)}{(T_{w,4} - T_s)(T_{w,3} + T_s)} - 2\left(\arctan\frac{T_{w,3}}{T_s} - \arctan\frac{T_{w,4}}{T_s}\right)\right]\right\} \quad \text{(B4)}$$

where the wall temperature T_w at any point along the tube is related to the gas temperature T by

$$T = T_w + \frac{\sigma\epsilon}{h_R}\left(T_w^4 - T_s^4\right) \quad \text{(B5)}$$

A numerical technique is required in the determination of the local wall temperature.

The total heat rejected from the radiator is equal to the heat lost by the gas flowing through it and is given by

$$Q_{rad} = wC_p(T_3 - T_4) \quad \text{(B6)}$$

APPENDIX C

PRESSURE RELATIONS

Fixed Cycle Loss Pressure Ratio

The cycle loss pressure ratio r_T/r_C is defined as (ref. 1)

$$\frac{r_T}{r_C} = \frac{\frac{P_1}{P_2}}{\frac{P_5}{P_4}} \tag{C1}$$

However,

$$P_5 = P_1 + (\Delta P)_h \tag{C2}$$

and

$$P_4 = P_2 - (\Delta P)_c \tag{C3}$$

where $(\Delta P)_h$ is the hot-side pressure loss or the pressure loss through the recuperator and heat source, and $(\Delta P)_c$ is the cold-side pressure loss or the pressure drop through the radiator and recuperator. Therefore,

$$\frac{r_T}{r_C} = \frac{\left[1 - \frac{(\Delta P)_c}{P_2}\right]}{\left[1 + \frac{(\Delta P)_h}{P_1}\right]} \tag{C4}$$

Because the turbine inlet pressure P_1 will be assumed fixed in this analysis, equation (C4) can be written as,

$$\frac{r_T}{r_C} = \frac{\left[1 - \frac{\Delta P_c}{P_1}\left(\frac{P_1}{P_2}\right)\right]}{\left[1 + \frac{(\Delta P)_h}{P_1}\right]} \tag{C5}$$

To enable the pressure drop through the radiator to be related to the cycle loss pressure ratio, the pressure drop in the radiator will be expressed as some fraction of the total pressure drop through the heat-transfer components in the cycle by the equation

$$K_1 \equiv \frac{(\Delta P)_{rad}}{(\Delta P)_{tot}} \tag{C6}$$

In addition, the pressure through the low-pressure side of the recuperator, $(\Delta P)_{rec}$ will be expressed as some constant fraction of the total cold-side pressure drop $(\Delta P)_c$, such that

$$K_2 = \frac{(\Delta P)_{rec}}{(\Delta P)_c} = \frac{(\Delta P)_{rec}}{(\Delta P)_{rec} + (\Delta P)_{rad}} \tag{C7}$$

The parameters K_1 and K_2 as defined are not totally independent of each another. Once the value of K_2 is fixed, K_1 has an upper bound. This upper bound is obtained from the assumption of no pressure loss through either the high-pressure side of the recuperator or the heat source, and is found to be

$$K_1 = 1 - K_2 \tag{C8}$$

If it is assumed that the pressure losses through both the high- and low-pressure sides of the recuperator are the same, then the upper bound on K_1 is further reduced and is given by

$$K_1 = 1 - \frac{2K_2}{1 + K_2} \tag{C9}$$

based on no pressure losses in the heat source.

Since, by definition

$$(\Delta P)_c = (\Delta P)_{rec} + (\Delta P)_{rad} \tag{C10}$$

equation (C7) becomes

$$(\Delta P)_{rec} = \frac{K_2}{1 - K_2} \tag{C11}$$

Using equations (C10) and (C11) and the equation

$$(\Delta P)_{tot} = (\Delta P)_h + (\Delta P)_c \tag{C12}$$

yields a rewritten form of equation (C6)

$$\frac{(\Delta P)_{rad}}{(\Delta P)_h + (\Delta P)_{rad}\left(\frac{K_2}{1 - K_2} + 1\right)} = K_1 \tag{C13}$$

or

$$\Delta P_h = \frac{(\Delta P)_{rad}}{K_1}\left(1 - \frac{K_1 K_2}{1 - K_2} - K_1\right) \tag{C14}$$

It now remains to relate $(\Delta P)_{rad}$ to the cycle loss pressure ratio of equation (C5). Substituting equations (C7), (C11), and (C14) into equation (C5) results in

$$\frac{r_T}{r_C} = \frac{1 - \left(\frac{1}{1 - K_2}\right)\left[\frac{(\Delta P)_{rad}}{P_1}\left(\frac{P_1}{P_2}\right)\right]}{1 + \left(\frac{1}{K_1} - \frac{K_2}{1 - K_2} - 1\right)\left[\frac{(\Delta P)_{rad}}{P_1}\right]} \tag{C15}$$

Rearranging and simplifying equation (C15) yield

$$(\Delta P)_{rad} = \frac{\left(1 - \frac{r_T}{r_c}\right)(1 - K_2)P_1}{\frac{r_T}{r_C}\left[\frac{(1 - K_2 - K_1)}{K_1}\right] + \frac{P_1}{P_2}} \tag{C16}$$

where P_1 is fixed, P_1/P_2, the turbine pressure, is given (ref. 1) as

$$\frac{P_1}{P_2} = \left[1 - \frac{1}{\eta_T}\left(1 - \frac{T_2}{T_1}\right)\right]^{-(\gamma/\gamma-1)} \tag{C17}$$

r_T/r_C is prescribed, and K_1 and K_2 can be parametrically varied within the limitation imposed by their definitions.

Fixed Component Pressure Loss

The radiator pressure-drop fraction, K_1 can also be related to the cycle loss pressure ratio r_T/r_C in terms of a fixed value of pressure loss for all the other heat-transfer components, $(\Delta P)_{comp}$. Because $(\Delta P)_{comp}$ is equal to $\left[(\Delta P)_{tot} - (\Delta P)_{rad}\right]$ by using equation (C6)

$$(\Delta P)_{comp} = \left(\frac{1 - K_1}{K_1}\right)(\Delta P)_{rad} \tag{C17}$$

If a fixed value of K_2 is also prescribed, the combination of equations (C13) and (C17) gives

$$\frac{r_T}{r_C} = \frac{1 - \frac{1}{(1 - K_2)}\frac{(\Delta P)_{comp}}{P_2}\frac{K_1}{1 - K_1}}{1 + \left(\frac{1}{K_1} - \frac{K_2}{1 - K_2} - 1\right)\frac{(\Delta P)_{comp}}{P_1}\frac{K_1}{1 - K_1}}$$

and in terms of $(\Delta P)_{comp}/P_1$

$$\frac{r_T}{r_C} = \frac{(1 - K_2)\left(\frac{1 - K_1}{K_1}\right) - \frac{P_1}{P_2}\left[\frac{(\Delta P)_{comp}}{P_1}\right]}{(1 - K_2)\left(\frac{1 - K_1}{K_1}\right)\left[1 + \frac{(\Delta P)_{comp}}{P_1}\right] - K_2\left[\frac{(\Delta P)_{comp}}{P_1}\right]} \tag{C18}$$

Thus, if $(\Delta P)_{comp}$ is specified, the contribution of the radiator pressure-drop variation K_1 to the cycle loss pressure ratio, and therefore to the cycle efficiency, can be evaluated from equation (C18). The maximum value of the cycle loss pressure ratio for a fixed value of $(\Delta P)_{comp}/P_1$ can be determined from equation (C18) by allowing K_1 to approach 0 and can be shown to be

$$\frac{r_T}{r_C} = \frac{1}{1 + \frac{(\Delta P)_{comp}}{P_1}} \tag{C19}$$

Local Pressures

If the turbine inlet pressure P_1 is prescribed, the pressure at every other point in the cycle can be expressed in terms of $(\Delta P)_{rad}$, K_1, and K_2.

The pressure at turbine outlet P_2 is given by equation (C15). The pressure at the radiator inlet is given by

$$P_3 = P_2 - \left(\frac{K_2}{1 - K_2}\right)(\Delta P)_{rad} \tag{C20}$$

At the inlet to the compressor, the pressure is

$$P_4 = P_3 - (\Delta P)_{rad} \tag{C21}$$

and, at the recuperator high-pressure inlet, the pressure is

$$P_5 = P_1 + \left(\frac{1}{K_1} - \frac{K_2}{1 - K_2} - 1\right)(\Delta P)_{rad} \tag{C22}$$

Finally, if it is assumed that the pressure drop through high-pressure side of the recuperator is the same as through the low-pressure side, the pressure at the inlet of the heat source can be expressed as

$$P_6 = P_1 + \frac{(1 - K_2) - K_1 - K_1K_2}{K_1(1 - K_2)} (\Delta P)_{rad} \tag{C23}$$

For the limiting case of no pressure losses through either the high-pressure side of the recuperator or through the heat source, $P_6 = P_5 = P_1$.

Pressure Drop Equation

The pressure drop in the radiator consists of losses through the headers and the radiator tubes. When it is assumed that the pressure drop through the headers is small in comparison with that through the radiator tubes and if entrance, bend, and fitting losses in the radiator are neglected, the pressure drop can be expressed by the Fanning equation. Thus,

$$(\Delta P)_{rad} = 2f_g\left(\frac{L}{D_i}\right)V_g^2 \frac{\rho_g}{g_c} \tag{C24}$$

Because the temperatures and pressure vary along the radiator tube, V_g and f_g must be taken as average values to obtain $(\Delta P)_{rad}$. The product $\rho_g V_g$ however, is a constant along the tube. For a gas-solid suspension, equation (C24) is modified to give

$$(\Delta P)_{rad} = 2f'_s\left(\frac{L}{D_i}\right)V_s^2 \frac{\rho_g}{g_c} \tag{C25}$$

where f'_s is the effective friction factor of the suspension and V_s is velocity of the suspension. Since in dilute suspensions the volume of solids is small compared with the volume of the gas, it can be assumed that V_s can be taken to be the same as the velocity of the gas phase V_g. Furthermore, the suspension-friction factor can be expressed as

$$f'_s = \left(\frac{f'_s}{f_g}\right)f_g \tag{C26}$$

where f_g is evaluated at the same gas-state conditions (V, P, T, D_i) as the suspension. Thus, equation (C25) becomes,

$$(\Delta P)_{rad} = 2\left(\frac{f'_s}{f_g}\right) f_g \left(\frac{L}{D_i}\right) V_g^2 \frac{\rho_g}{g_c} \tag{C27}$$

The friction-factor ratio f'_s/f_g is assumed to be adequately represented by the relation

$$\frac{f'_s}{f_g} = 1 + 4.0(Re)_g^{-0.32}\,\eta \tag{C28}$$

presented in reference 5.

For fully developed turbulent flow in smooth pipes (e.g., ref. 8),

$$f_g = 0.046(Re)_g^{-0.2} \tag{C29}$$

where

$$(Re)_g = \frac{D_i \rho_g V_g}{\mu_g} = \frac{D_i G_g}{\mu_g} \tag{C30}$$

If it can be assumed that the gas flow is essentially incompressible (there is a question as to what the effective sonic velocity of a suspension is), then the gas phase static density is related to the local gas total pressure and temperature by the equation

$$\rho_g = \frac{P}{R'T} \tag{C31}$$

and the velocity at any point in the radiator tube is given by

$$V_g = \frac{G_g R'T}{P} \tag{C32}$$

Because equation (C27) requires an effective average velocity, equation (C32) can be expressed in terms of the inlet velocity ($P = P_3$ and $T = T_3$) multiplied by a correction factor F derived in reference 7 as

$$F = 1.5\left[\frac{1 - \left(\frac{T_3}{T_4}\right)^2}{1 - \left(\frac{T_3}{T_4}\right)^3}\right] \tag{C33}$$

so that the effective average velocity is

$$\left(V_g\right)_{av} = \frac{FG_g R' T_3}{P_3} \tag{C34}$$

Thus equation (C27) becomes

$$(\Delta P)_{rad} = 2F\left[1 + 4.0(Re)_g^{-0.32}\eta\right]\left[0.046(Re)_g^{-0.2}\right]\frac{L}{D_i}\,\frac{G_g^2 R' T_3}{g_c P_3} \tag{C35}$$

The cycle calculations determine the total mass flow rate w which, in terms of the radiator model, is given for a pure gas by

$$w_g = \rho_g V_g \frac{\pi}{4} D_i^2 N \tag{C36}$$

and for a suspension by

$$w_s = \rho_s V_s \frac{\pi}{4} D_i^2 N \tag{C37}$$

For low values of the particle loading ratio ($\eta < 10$) the density of the suspension ρ_s is approximately equal to (see ref. 5)

$$\rho_s = \rho_g(1 + \eta) \tag{C38}$$

With the assumption that $V_s = V_g$, equation (C37) can be written as

$$w_s = (1 + \eta)\rho_g V_g \frac{\pi}{4} D_i^2 N \tag{C39}$$

so that G_g in equation (C35) can be obtained as

$$G_g = \frac{w_s}{(1 + \eta) \frac{\pi}{4} D_i^2 N} \tag{C40}$$

Combining equations (C40) and (C35) yields

$$(\Delta P)_{rad} = 2F\left[1 + 4.0(Re)_g^{-0.32}\eta\right]\left[0.046(Re)_g^{-0.2}\right]\left(\frac{L}{D_i}\right)\left(\frac{R'T_3}{g_c P_3}\right)\left[\frac{w_s}{(1 + \eta) \frac{\pi}{4} D_i^2 N}\right]^2 \tag{C41}$$

where $(Re)_g$ is given by,

$$(Re)_g = \frac{w_s}{\mu(1 + \eta) \frac{\pi}{4} D_i N} \tag{C42}$$

The radiator pressure drop can thus be related to the radiator geometry, the radiator flow Reynolds number, and the cycle mass flow rate.

APPENDIX D

COMPUTATIONAL PROCEDURE

All cycle and radiator model computations were performed on the IBM 7094 computer at the Lewis Research Center. The procedure used for the computation is outlined herein,

(1) The gas Reynolds number is set (this number can be varied parametrically).

(2) The cycle loss pressure ratio r_T/r_C is set (this number can also be varied parametrically if desired).

(3) The properties of the working fluid are set by feeding in the appropriate data from appendix E (depending upon whether a pure gas or a gas-graphite suspension is used). If a suspension is considered, the values of η and δ are varied parametrically.

(4) The pressure drop across the radiator is calculated using equation (C14) for the specified value of the cycle loss pressure ratio and the prescribed values of K_1, K_2, and P_1, and P_1/P_2 obtained from equation (C15). The pressures at points 3 to 6 in the cycle (fig. 1) are calculated using equations (C20) to (C23), respectively. For the limiting case of K_1 given by equation (C8), P_5 and P_6 are taken to be the same as P_1.

(5) A value of the inside diameter of the tubes D_i is assumed, and h_R is computed from equation (23).

(6) Knowing h_R, r_T/r_C, and the specified cycle inputs as outlined previously, the cycle efficiency η_{cy}, the mass rate of flow w, and the radiator prime area A_p are computed (for each T_2/T_1 and T_4/T_1 considered) using equations (B1), (B3), and (B4), respectively. The temperatures at every point in the cycle are also determined.

(7) Because $(Re)_g$ is specified and A_p and w have been computed in step (6), equation (25) allows for the direct evaluation of L (the tube length), once l_f/D_o, D_o/D_i, and η_f are specified.

(8) The value of L is known from equation (25); therefore, D_i can be calculated using equation (24).

(9) The value of D_i computed in step (8) is compared with the value of D_i assumed in step (5). If the two values differ by more than 1 percent, steps (5) to (8) are repeated using the new value of D_i as the assumed value of D_i in step (5).

(10) When the new value of D_i is close enough to the previous trial to satisfy the specifications of the program, the gas mass velocity G_g is computed from equation (C30) and the number of tubes N is computed using equation (26).

After convergence of D_i has been achieved, the computer program prints out the prime area A_p, the inside diameter of the tubes D_i, the length of the tubes L, the number of tubes N, the pressure drop across the radiator $(\Delta P)_{rad}$, the mass flux of the

gas in each G_g, the tube Reynolds number of the gas $(Re)_g$, the heat-transfer coefficient h_R, the planform area A_{pl}, the vulnerable area A_v, and the average velocity through the tubes V_{av}. The program also prints out all cycle variables and input parameters including T_1, T_2/T_1, T_s, η_C, η_T, r_T/r_C, γ_s, ϵ, T_4/T_1, δ, η, $T_{w,4}$, wC_p/P_s, F, T_3/T_1, $T_{w,3}$, T_6/T_1, T_5/T_1, η_{cy}, and A_p/P_s, as well as the pressures at each point in the cycle P_1, P_2, P_3, P_4, P_5, and P_6, and the pressure ratio across the turbine P_1/P_2.

APPENDIX E

PROPERTIES OF GASES

The values and equations for the gas properties used as inputs to the computer program are listed herein. The equations were obtained from faired curves based on the data of reference 10 in the temperature range from 760° to 1960° R (422 to 1090 K). The viscosity and thermal conductivity values were determined at the arithmetic mean temperature in the radiator.

Property	U.S. customary units	SI units
	Helium	
C_p	1.25 Btu/(lb mass)($^{\circ}$R)	5230 J/(kg)(K)
γ	1.67	1.67
R'	386.25 (lb force/lb mass)(ft/$^{\circ}$R)	2080 J/(kg)(K)
k	$0.433\ T^{0.650} \times 10^{-5}$ Btu/(sec)(ft)($^{\circ}$R)	$0.33\ T^{0.650} \times 10^{-2}$ J/(sec)(m)(K)
μ	$0.0238\ T^{0.650} \times 10^{-5}$ lb mass/(ft)(sec)	$0.0519\ T^{0.650} \times 10^{-5}$ (N)(sec)/m^2
	Neon	
C_p	0.25 Btu/(lb mass)($^{\circ}$R)	1046 J/(kg)(K)
γ	1.67	1.67
R'	77.25 (lb force/lb mass)(ft/$^{\circ}$R)	416 J/(kg)(K)
k	$0.0128\ T^{0.662} \times 10^{-5}$ Btu/(sec)(ft)($^{\circ}$R)	$0.0098\ T^{0.662} \times 10^{-2}$ J/(sec)(m)(K)
μ	$0.0232\ T^{0.665} \times 10^{-5}$ lb mass/(ft)(sec)	$0.0509\ T^{0.665} \times 10^{-5}$ (N)(sec)/m^2
	Argon	
C_p	0.125 Btu/(lb mass)($^{\circ}$R)	523 J/(kg)(K)
γ	1.67	1.67
R'	38.63 (lb force/lb mass)(ft/$^{\circ}$R)	208 J/(kg)(K)
k	$0.00298\ T^{0.725} \times 10^{-5}$ Btu/(sec)(ft)($^{\circ}$R)	$0.237\ T^{0.725} \times 10^{-5}$ J/(sec)(m)(K)
μ	$0.0156\ T^{0.665} \times 10^{-5}$ lb mass/(ft)(sec)	$0.0355\ T^{0.725} \times 10^{-5}$ (N)(sec)/m^2

The only property of graphite used as an input to the computer program is its specific heat. This value over the temperature range 500° to 2000° R (278 to 1112 K) was taken as 0.39 Btu per pound mass per $^{\circ}$R (1635 J/(kg)(K)). Therefore, the values of δ, which were used, are:

Suspension	Particle to gas specific heat ratio, δ
Helium-graphite	0.312
Neon-graphite	1.56
Argon-graphite	3.12

It was also assumed that the average diameter of the graphite particles was of the order of 30 micrometers.

APPENDIX F

RADIATOR WEIGHT

For the radiator fin-tube model of figure 5, the weight of the radiator panels composed of fins and tubes is given by

$$W = NL\left[\frac{\pi}{4}\left(D_o^2 - D_i^2\right)\rho_t + 2l_f t_f \rho_f\right] \tag{F1}$$

or in terms of ratios

$$W = \rho_t NLD_i^2\left(\frac{D_o}{D_i}\right)^2\left\{\frac{\pi}{4}\left[1 - \left(\frac{D_i}{D_o}\right)^2\right] + 2\left(\frac{\rho_f}{\rho_t}\right)\left(\frac{l_f}{D_o}\right)\left(\frac{t_f}{D_o}\right)\right\} \tag{F2}$$

Now, the planform area is given by

$$A_{pl} = NLD_i\left(\frac{D_o}{D_i}\right)\left(1 + 2\,\frac{l_f}{D_o}\right) \tag{F3}$$

Substituting in equation (F2) yields

$$W = \rho_t A_{pl} D_i\left(\frac{D_o}{D_i}\right)\left(1 + 2\,\frac{l_f}{D_o}\right)\left\{\frac{\pi}{4}\left[1 - \left(\frac{D_i}{D_o}\right)^2\right] + 2\left(\frac{\rho_f}{\rho_t}\right)\left(\frac{l_f}{D_o}\right)\left(\frac{t_f}{D_o}\right)\right\} \tag{F4}$$

Thus, with ρ_t and l_f/D_o taken as the same for both the suspension and pure-gas radiators, the weight ratio becomes

$$\frac{W_s}{W_g} = \frac{\left(A_{pl}\right)_s}{\left(A_{pl}\right)_g}\frac{\left(D_i\right)_s}{\left(D_i\right)_g}\frac{\left(\frac{D_o}{D_i}\right)_s}{\left(\frac{D_o}{D_i}\right)_g}\left\{\frac{\frac{\pi}{4}\left[1 - \left(\frac{D_i}{D_o}\right)_g^2\frac{\left(\frac{D_o}{D_i}\right)_g^2}{\left(\frac{D_o}{D_i}\right)_s^2}\right] + 2\left(\frac{\rho_f}{\rho_t}\right)_s\left(\frac{l_f}{D_o}\right)_s\left(\frac{t_f}{D_o}\right)_s}{\frac{\pi}{4}\left[1 - \left(\frac{D_i}{D_o}\right)_g^2\right] + 2\left(\frac{\rho_f}{\rho_t}\right)_g\left(\frac{l_f}{D_o}\right)_g\left(\frac{t_f}{D_o}\right)_g}\right\} \tag{F5}$$

In equation (F5), it is assumed that the parameters ρ_f/ρ_t, l_f/D_o, and t_f/D_o remain the same for the suspension and pure-gas cases. Furthermore, for the prescribed radiator model, $(D_o/D_i)_g = 1.33$ and $l_f/D_o = 3.5$. Thus, with values of $(A_{pl})_s/(A_{pl})_g$ and $(D_i)_s/(D_i)_g$ obtained from the previous calculation results (e.g., figs. 24, 25, 27, and 30), values of the weight ratio can be obtained as a function of the ratio $(D_o/D_i)_s/(D_o/D_i)_g$ for parametric values of t_f/D_o and ρ_f/ρ_t for any desired basis of comparison (e.g., same Reynolds number, same panel aspect ratio, etc.). Two values of ρ_f/ρ_t equal to 0.34 and 1.0 were chosen to represent either fins and tubes of the same material or aluminum fins with stainless-steel tubes.

Realistic values of $(D_o/D_i)_s$ can be obtained from the calculation results for the criterion of equal meteoroid protection. According to meteoroid protection theory, the required tube wall thickness is given by

$$t_t = \frac{\text{Constant}}{(E_t\rho_t)^{1/2}}\left(\frac{A_v\tau}{-\ln P(O)_t}\right)^{0.25} \tag{F6}$$

where E_t is the modulus of elasticity of the tube material, ρ_t is the density of the tube material, A_v is the vulnerable area of the radiator panel, τ is the design lifetime of the radiator, and $P(O)_t$ is the probability of no puncture during the lifetime of the radiator. The tube wall thickness can also be expressed as

$$t_t = \frac{1}{2}D_i\left(\frac{D_o}{D_i} - 1\right) \tag{F7}$$

so that taking the ratio of suspension-case tube thickness to pure-gas-case tube thickness (from eqs. (F6) and (F7)) results in

$$\left(\frac{D_{i,s}}{D_{i,g}}\right)\left[\frac{\left(\frac{D_o}{D_i}\right)_s - 1}{\left(\frac{D_o}{D_i}\right)_g - 1}\right] = \left[\frac{(A_v)_s}{(A_v)_g}\right]^{0.25} \tag{F8}$$

where E_t, ρ_t, τ, and $P(O)_t$ are the same for both cases.

The vulnerable area of the radiator is given by

$$A_v = \pi D_o LN \tag{F9}$$

From the definition of radiator planform area (eq. (F3)),

$$A_v = A_{pl}\left[\frac{\pi}{1 + 2\left(\frac{l_f}{D_o}\right)}\right] \tag{F10}$$

Substitution of equation (F10) into equation (F8) with l_f/D_o taken the same in both cases, yields the expression for tube diameter ratio for the suspension case for equal meteoroid protection

$$\left(\frac{D_o}{D_i}\right)_s = 1 + \frac{\left(\frac{D_o}{D_i}\right)_g - 1}{\frac{(D_i)_s}{(D_i)_g}}\left[\frac{(A_{pl})_s}{(A_{pl})_g}\right]^{0.25} \tag{F11}$$

In equation (F11), $(D_i)_s/(D_i)_g$ and $(A_{pl})_s/(A_{pl})_g$ are obtained from the calculated results for the particular basis of comparison desired, while $(D_o/D_i)_g = 1.33$ for the pure-gas model.

REFERENCES

1. Glassman, Arthur J.; and Stewart, Warner L.: Thermodynamic Characteristics of Brayton Cycles for Space Power. J. Spacecraft Rockets, vol. 1, no. 1, Jan.-Feb. 1964, pp. 25-31.

2. Stewart, Warner L.; Glassman, Arthur J.; and Krebs, Richard P.: The Brayton Cycle for Space Power. Paper No. 741A, SAE, Sept. 1963.

3. Glassman, A. J.; Krebs, R. P.; and Fox, T. A.: Brayton Cycle Nuclear Space Power Systems and Their Heat-Transfer Components. AIChE Chem. Eng. Progr. Symp. Ser., vol. 61, no. 57, 1965, pp. 306-314.

4. Norman, L. W.: The Application of the Recuperated Brayton Cycle to Space Power Conversion Systems. Paper No. 63-220, AIAA, June 1963.

5. Pfeffer, Robert; Rossetti, Salvatore; and Lieblein, Seymour: Analysis and Correlation of Heat-Transfer Coefficient and Friction Factor Data for Dilute Gas-Solid Suspensions. NASA TN D-3603, 1966.

6. Barthelemy, P.; Chauvineau, C.; and Dieulot, G.: Thermodynamics of the Brayton Cycle for Space Applications. Rep. No. YCP-471, Sixieme Colloque AGARD, Paris, 1963.

7. Saule, Arthur V.; Krebs, Richard P.; and Auer, Bruce M.: Design Analysis and General Characteristics of Flat-Plate Central-Fin-Tube Sensible-Heat Space Radiators. NASA TN D-2839, 1965.

8. Foust, Allan S.; Wenzel, Leonard A.; Clump, Curtis W.; Maus, Louis; and Anderson, L. Bryce: Principles of Unit Operations. John Wiley & Sons, Inc., 1960.

9. Stockman, Norbert O.; Bittner, Edward C.; and Sprague, Earl L.: Comparison of One- and Two-Dimensional Heat-Transfer Calculations in Central Fin-Tube Radiators. NASA TN D-3645, 1966.

10. Svehla, Roger A.: Estimated Viscosities and Thermal Conductivities of Gases at High Temperatures. NASA TR R-132, 1962.

NASA-Langley, 1968 —— 3 E-3602

NATIONAL AERONAUTICS AND SPACE ADMINISTRATION
WASHINGTON, D. C. 20546

OFFICIAL BUSINESS

POSTAGE AND FEES PAID
NATIONAL AERONAUTICS AND
SPACE ADMINISTRATION

FIRST CLASS MAIL

"The aeronautical and space activities of the United States shall be conducted so as to contribute . . . to the expansion of human knowledge of phenomena in the atmosphere and space. The Administration shall provide for the widest practicable and appropriate dissemination of information concerning its activities and the results thereof."

—NATIONAL AERONAUTICS AND SPACE ACT OF 1958

NASA SCIENTIFIC AND TECHNICAL PUBLICATIONS

TECHNICAL REPORTS: Scientific and technical information considered important, complete, and a lasting contribution to existing knowledge.

TECHNICAL NOTES: Information less broad in scope but nevertheless of importance as a contribution to existing knowledge.

TECHNICAL MEMORANDUMS: Information receiving limited distribution because of preliminary data, security classification, or other reasons.

CONTRACTOR REPORTS: Scientific and technical information generated under a NASA contract or grant and considered an important contribution to existing knowledge.

TECHNICAL TRANSLATIONS: Information published in a foreign language considered to merit NASA distribution in English.

SPECIAL PUBLICATIONS: Information derived from or of value to NASA activities. Publications include conference proceedings, monographs, data compilations, handbooks, sourcebooks, and special bibliographies.

TECHNOLOGY UTILIZATION PUBLICATIONS: Information on technology used by NASA that may be of particular interest in commercial and other non-aerospace applications. Publications include Tech Briefs, Technology Utilization Reports and Notes, and Technology Surveys.

Details on the availability of these publications may be obtained from:

SCIENTIFIC AND TECHNICAL INFORMATION DIVISION

NATIONAL AERONAUTICS AND SPACE ADMINISTRATION

Washington, D.C. 20546